PCCP

ROYAL SOCIETY OF CHEMISTRY

PERSPECTIVE

View Article Online
View Journal | View Issue

Cite this: *Phys. Chem. Chem. Phys.*, 2023, **25**, 32778

The high resolution absorption spectrum of methane in the 10 800–14 000 cm^{-1} region: literature review, new results and perspectives†

A. Campargue, *[a] E. V. Karlovets,[b] S. S. Vasilchenko[c] and M. Turbet[d]

The recent development of high resolution spectrographs for exoplanetary research in the visible range makes suitable an improvement of our knowledge of the high resolution spectrum of methane. In this contribution, the weak and highly congested absorption spectrum of methane in the 10 800–14 000 cm^{-1} region (0.71–0.93 μm) is considered on the basis of (i) an exhaustive review of the literature over the lasts decades, (ii) the analysis of a spectrum recorded at Kitt Peak by Fourier transform spectroscopy at room temperature, (iii) a very high sensitivity spectrum recorded by cavity ring down spectroscopy near 760 nm. The line list retrieved from the Kitt Peak spectrum includes 12 800 lines between 10 802 and 13 922 cm^{-1}. Together with the CRDS line list in the 13 060–13 300 cm^{-1} interval (about 2650 lines), the reported FTS dataset represents the first high resolution extensive intensity measurements of methane for wavenumbers above 11 502 cm^{-1}. A very good agreement between our Kitt Peak line list and HITRAN list is found in the 10 800–11 502 cm^{-1} interval. The "quasi-continuum" absorption background underlying the congested spectrum around 11 200 cm^{-1} is quantitatively evaluated to about 42% of the absorption by CH_4 lines. Previous laser-based investigations are critically reviewed by comparison to the FTS and CRDS experimental data retrieved in the present work. The review of the studies of the minor isotopologues ($^{13}CH_4$, CH_3D, CH_2D_2, and CHD_3) is also presented. Intensity comparison with band models used for planetary applications is discussed and confirms the importance of the "quasi-continuum" absorption in the methane spectrum at room temperature. The comparison to the TheoReTs line list obtained by *ab initio* calculations gives valuable hints for future assignments but the TheoReTS line positions are not sufficiently accurate for application to high resolution exoplanetary spectra in the region. From the various comparisons and results obtained in this work, we conclude that the high frequency absorption spectrum of methane deserves to be revisited by modern cavity-enhanced absorption techniques to fulfil needs both for future analysis of high resolution exoplanetary spectra and for theoretical analysis.

Received 24th May 2023,
Accepted 9th November 2023

DOI: 10.1039/d3cp02385k

rsc.li/pccp

1. Introduction

Producing reliable spectroscopic databases of methane and any other molecule of interest in the visible wavelengths is essential to search for these molecules in the atmosphere of exoplanets. This is particularly critical for observations in reflected light, which is maximal in the visible where the peak of the stellar blackbody lies. We have today at our disposal several visible light high-resolution spectrographs (resolving power $R = \lambda/\Delta\lambda = \sigma/\Delta\sigma \sim 100\,000$–$200\,000$) such as VLT@ESPRESSO,[1] in a few years VLT@RISTRETTO,[2] and in the longer term E-ELT@ANDES.[3] These spectrographs have in principle the capability to detect molecules absorbing in the visible (*e.g.* H_2O, O_2, and also CH_4). While molecular detection attempts have already been made in the visible with the ESPRESSO spectrograph for hot giant exoplanets,[4,5] in particular for the H_2O molecule, CH_4 is for the moment inaccessible at these wavelengths because the techniques used require precise knowledge of the properties of the CH_4 lines (in particular, of the line positions) in the visible, which is not the case yet. The method used indeed consists in cross-correlating the observed astrophysical signal (obtained by

[a] *University Grenoble Alpes, CNRS, LIPhy, 38000 Grenoble, France. E-mail: Alain.Campargue@univ-grenoble-alpes.fr*
[b] *Tomsk State University, Department of Optics and Spectroscopy, 36, Lenin Avenue, 634050, Tomsk, Russia*
[c] *V.E. Zuev Institute of Atmospheric Optics, 1, Academician Zuev Square, 634055 Tomsk, Russia*
[d] *Laboratoire de Météorologie Dynamique/IPSL, CNRS, Sorbonne Université, École Normale Supérieure, Université PSL, Ecole Polytechnique, Institut Polytechnique de Paris, 75005 Paris, France*

† Electronic supplementary information (ESI) available. See DOI: https://doi.org/10.1039/d3cp02385k

transit, emission or reflected light spectroscopy) with a simulated spectrum containing the lines of the molecule which one seeks to detect.[6–8] A prerequisite of the method is thus a precise knowledge of at least the position of the strongest lines (to generate a binary mask) and optimally of all the other properties of the lines (to generate more realistic simulated spectra).

Our ability to detect CH_4 in the visible is particularly interesting in the context of atmospheric characterization of nearby temperate rocky exoplanets such as Proxima b,[9] which will soon be the targets of the RISTRETTO and ANDES spectrographs *via* their reflected light. Methane is particularly interesting because with O_2 (with strong detectable features in the visible – see *e.g.* ref. 10), it is a pair of molecules of astrobiological interest.[11,12]

The methane spectrum consists in a series of strong absorption spectral structures separated by about 1500 cm^{-1} with intensity decreasing by about one order of magnitude every 3000 cm^{-1}. This general appearance results from approximate relations between the vibrational frequencies, $\nu_1 \approx \nu_3 \approx 2\nu_2 \approx 2\nu_4 \approx 3000$ cm^{-1}, which leads to very close energies for vibrational states having the same polyad number $P = 2(V_1+V_3)+V_2+V_4$, where V_i are the normal mode vibrational quantum numbers.[13] (The ν_1 and ν_3 stretching modes correspond to frequencies of 2916 and 3019 cm^{-1}, respectively while the ν_2 and ν_4 bending modes have a 1533 and 1311 cm^{-1} frequency, respectively.) Each strong absorbing region is thus associated to bands reaching vibrational levels belonging to a same polyad of interacting vibrational states. In spite of its small number of atoms and high symmetry, at high spectral resolution, the number and strength of the rovibrational interactions lead to a general disappearance of regular spectral structures and a considerable spectral congestion increasing, in the near infrared and visible regions. As a result, rovibrational assignments and theoretical interpretation of methane spectra are practically absent above 8000 cm^{-1} and measured transitions are provided in spectroscopic databases with experimental line parameters and scarce rovibrational assignments.[13–15]

The overview of the HITRAN line list above 9500 cm^{-1} is included in Fig. 1. It is limited to two empirical line lists in the 9500–10 500 cm^{-1} and 11 000–11 500 cm^{-1} intervals (P = 7 and 8, respectively) obtained by long pathlength Fourier transforms spectroscopy (FTS)[16] and high sensitivity intracavity laser absorption spectroscopy (ICLAS),[17] respectively. As mentioned above, the development and use of visible light high-resolution spectrographs for methane detection in exoplanetary atmospheres make it necessary to characterize the high resolution spectrum of methane towards higher energies, in the visible range.

The aim of the present work was initially to review the high resolution laboratory studies of methane available in the literature above 10 000 cm^{-1}, in support of exoplanetary applications. In the review process, it appeared that a room temperature methane FTS spectrum available in the Kitt Peak archives (ref. 930825R0.004) has sufficient sensitivity to exhibit absorption lines up to 14 000 cm^{-1} and was thus worth to analyze. This spectrum presented in Fig. 1 was recorded in 1993 with a pathlength of 73 m and a CH_4 pressure of 99.8 Torr

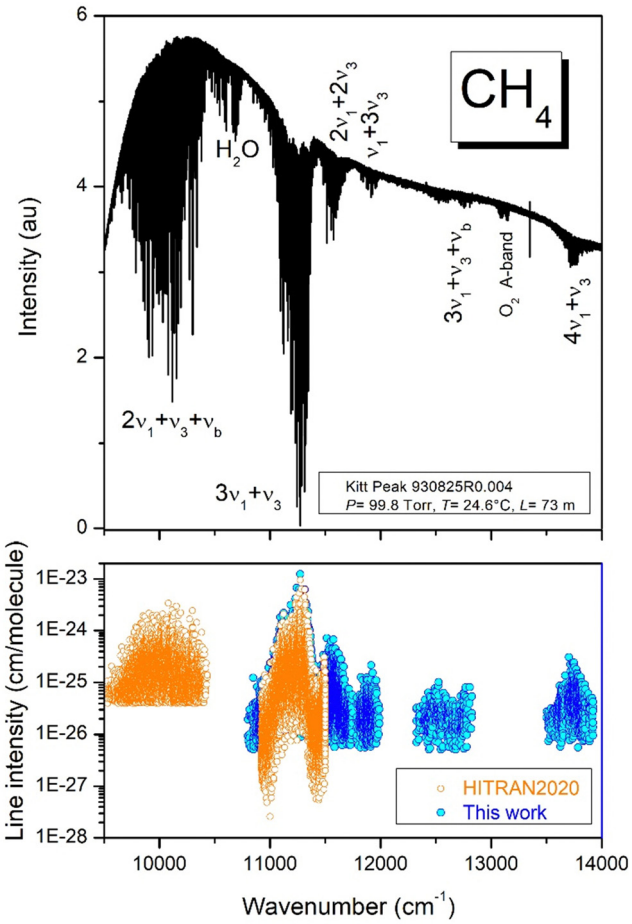

Fig. 1 Upper panel: Raw FTS spectrum of the methane room temperature spectrum recorded at Kitt Peak (ref. 930825R0.004) between 9500 and 14 000 cm^{-1} (P = 98.8 Torr, l = 73.0 m, T = 297.7 K). Lower panel: Overview of the corresponding line list retrieved in this work above 10 800 cm^{-1} (blue circles) and comparison to the HITRAN list of methane[15] (orange circles).

(13 200 Pa) allowing for the detection of weak lines with an intensity down to 5×10^{-27} cm per molecule.

In the following section, we will present the line list retrieval from this Kitt Peak (KP) spectrum above 10 800 cm^{-1} (the 11 000–11 500 cm^{-1} interval overlapping with the HITRAN list will be used for validation tests). In Section 3, we will present a very high sensitivity spectrum of methane newly recorded in Tomsk by cavity ring down spectroscopy (CRDS) in the 13 060–13 300 cm^{-1} interval where methane absorption lines are very weak. Then, in Section 4, the literature about high resolution laboratory data in the 10 800–14 000 cm^{-1} interval will be systematically reviewed. Starting from grating spectrograph with photographic plate detection,[18,19] several high sensitivity absorption methods were implemented to measure the weak methane spectrum, sometimes at low temperatures (77 K or in jet cooled conditions): wavelength modulation diode laser spectroscopy (WMDLS), photoacoustic spectroscopy (PAS), ICLAS, laser-induced grating spectroscopy (LIGS). When possible, we will compare our KP line list in relation with these previous works. Section 4 will also include a literature review

for the high resolution studies of the minor isotopologues ($^{13}CH_4$, CH_3D, CH_2D_2, and CHD_3). In Section 5, low resolution simulations will allow for a comparison to absorption coefficients used in planetology. In the final section, general conclusions will be drawn and perspectives will be presented considering the review of the experimental literature, the results obtained in the present work and the best-to-date theoretical calculations.

2. Analysis of the Kitt Peak spectrum

The spectrum under analysis (ref. 930825R0.004) was recorded at the National Solar Observatory at Kitt Peak in 1993. The methane pressure and absorption path length was 98.8 Torr and 73 m, respectively. The temperature of the recording was 24.6 °C (297.7 K). The noise level evaluated as the RMS of the absorbance in a region free of absorption lines is on the order of 2.5×10^{-3}, corresponding to a noise equivalent absorption of $\alpha_{min} \approx 3.4 \times 10^{-7}$ cm^{-1} and minimum line intensities of 5×10^{-27} cm per molecule. Fig. 2 shows an overview of the strongest band system near 11 300 cm^{-1} corresponding to the $3\nu_1 + \nu_3$ manifold ($P = 8$) with two successive zooms illustrating the spectral congestion and the achieved signal-to-noise ratio.

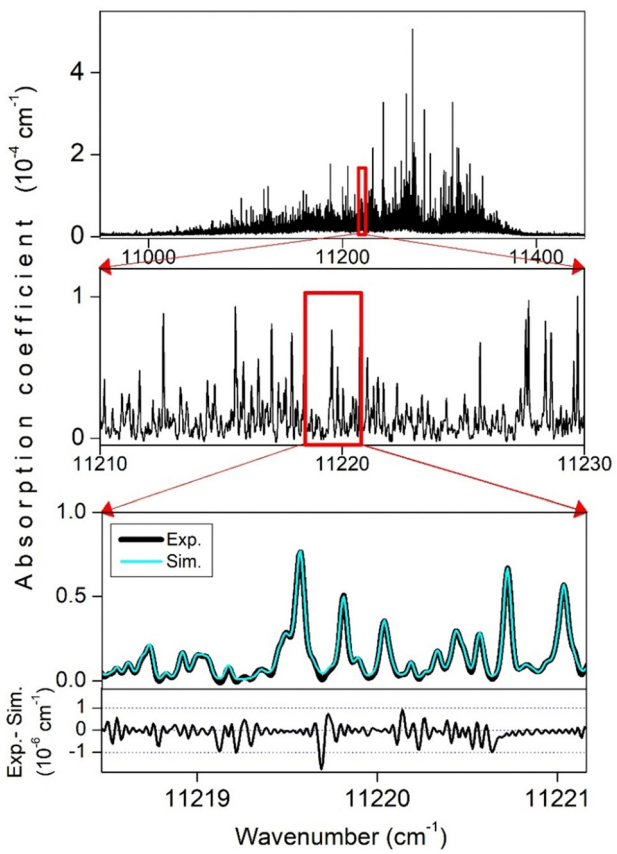

Fig. 2 FTS spectrum of the methane room temperature spectrum recorded at Kitt Peak (ref. 930825R0.004) near 11 300 cm^{-1} (P = 98.8 Torr, l = 73.0 m, T = 297.7 K). The two enlargements illustrate the spectral congestion. On the lower panel, the simulation (cyan) provided by a multiline fitting procedure is superimposed to the spectrum and the corresponding residuals are displayed.

2.1. Line list

As illustrated in Fig. 2, isolated lines are mostly absent and the important spectral congestion resulted in a laborious retrieval of the line centers and line intensities. An important difficulty is related to the baseline positioning. As visible on the overview spectrum presented on Fig. 1, in the region of the strong absorption near 11 300 cm^{-1} and to a lesser extend near 13 800 cm^{-1}, part of the absorption appears as a continuum and the apparent baseline does not correspond to the zero absorption. This is probably due to the accumulation of numerous unresolved weak lines together with a possible contribution of the wings of stronger lines which are slightly pressure broadened at P = 98.8 Torr. As the used fitting program cannot fit as a whole the thousands of lines contributing to the spectrum, the fit has to be performed sequentially by considering successive intervals involving a few tens of lines at maximum, which can be fitted simultaneously. In this process, the fitted local baseline is assumed to be a straight line, thus mostly ignores the weak underlying unresolved absorption. In other words, the resulting line list does not account for the continuous background which represents a significant part of the absorption in the two above-mentioned regions. At the end of the line parameter retrieval, the unresolved background absorption must be estimated and provided separately to account for the total absorption. The continuous background is obtained as illustrated in Fig. 3, by subtracting from the measured spectrum the absorption of the lines simulated using the constructed line list.

Let us give more details on the line parameter retrieval. A homemade three step suite of multiline fitting programs written in Labview and C++ was used to reproduce the spectrum (see Fig. 3 of ref. 16). Regarding the line shapes, we adopted a Voigt profile. Default values of the Gaussian and Lorentzian widths were determined from a fit of the profile of a small number of relatively isolated lines. (We obtained a Gaussian HWHM of 1.7×10^{-2} cm^{-1} corresponding to the Doppler width and the Lorentzian HWHM of 1.8×10^{-2} cm^{-1}.) A preliminary peak list (line centre, peak height) was obtained using a standard peak finder procedure and a synthetic spectrum was then simulated by attaching to each peak the default Voigt profile. Then a multiline fit was performed over the analysed spectral interval by adjusting only the line centre and integrated line absorbance, the shape of all the lines being fixed to the default Voigt profile. Finally, a manual adjustment was performed by further refining the profile parameters and adding/deleting weak lines when needed. In the case of highly blended features, we tried to limit the number of components and preferred to relax reasonably the constraints on the profile parameters than to add lines. The resulting list provided as ESI† is presented in Fig. 1. It includes a total of about 12 800 lines for the three following interval 10 802–11 988, 12 325–12 825 and 13 502–13 922 cm^{-1} (11 541, 455 and 842 lines respectively). The absence of lines due to water vapor

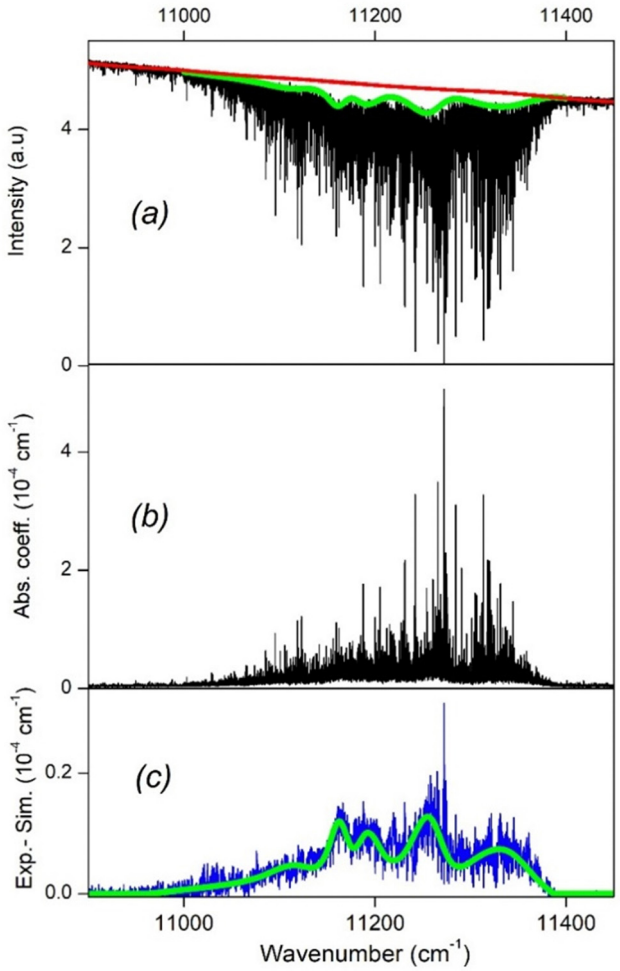

Fig. 3 The different steps of the retrieval of the background "continuum" in the 11 300 cm^{-1} region. In (a), the baseline is visually estimated (red line) and used to obtain the absorption coefficient displayed in (b). The absorption of the lines is simulated from the fitted values of the line parameters and subtracted from the experimental absorption coefficient, leading to the residuals displayed in (c) (blue curve). By smoothing the residuals, the background "continuum" is obtained (green line in (c) and (a)).

(which could have been present in the sample as an impurity) was checked.

2.2. Retrieval of the "continuum" background

Fig. 3 illustrates the different steps of the retrieval of the "continuum" background in the 11 300 cm^{-1} region. First, based on a large scale view of the spectrum (Fig. 1), the zero-absorption baseline, $I_0(\nu)$, was visually estimated and approximated by a straight line (Fig. 3a, red line). On the basis of this baseline, the absorption coefficient was calculated using the Beer–Lambert law, $\alpha(\nu) = \frac{1}{l}\ln\left[\frac{I_0(\nu)}{I(\nu)}\right]$ (Fig. 3b). The absorption coefficient due to the lines, $\alpha_{\text{lines}}(\nu)$, was then simulated using the line list, leading to the $[\alpha(\nu) - \alpha_{\text{lines}}(\nu)]$ residuals (blue line on Fig. 3c). These residuals were approximated by a smoothed curve (light green on Fig. 3c) accounting for the background "continuum", also shown on the recorded spectrum (Fig. 3a). For each wavenumber value between 11 000 and 11 400 cm^{-1}, we provide as ESI,† the values of the "continuum" absorption cross-section (in cm^2 per molecule), obtained by normalizing the residuals by the molecular density in the experimental conditions of the analyzed KP spectrum (P = 98.8 Torr, T = 297.7 K). This absorption "continuum" which represents about one third of the total absorption in the region, should be combined to the line list to account for the experimental spectrum.

Regarding uncertainties on the line positions, the frequency calibration of the spectrum was checked by comparison to the HITRAN database. About 80 positions of strong and well isolated lines were compared in the 11 300–11 500 cm^{-1} interval. The average position difference was found smaller than 2×10^{-4} cm^{-1} with a standard deviation of 4.42×10^{-4} cm^{-1}. Taking into account a possible small contribution of the self pressure shift, an uncertainty of 5×10^{-3} cm^{-1} is believed to be a conservative estimate of the error bar for most of our line positions (excluding highly blended and very weak lines).

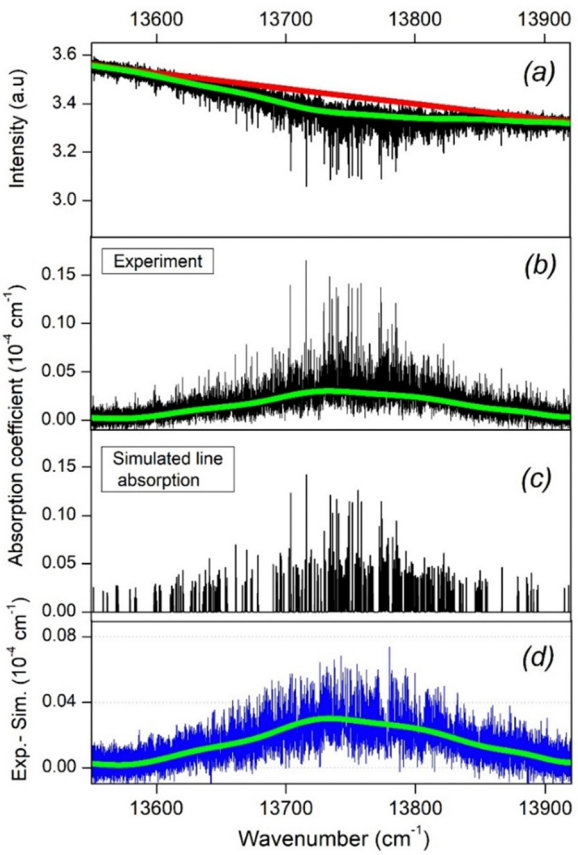

Fig. 4 Different steps of the retrieval of the background "continuum" in the 13 800 cm^{-1} region. In (a), the baseline is visually estimated (red line) and used to obtain the absorption coefficient displayed in (b). The absorption of the lines is simulated from the fitted values of the line parameters (c) and subtracted from the experimental absorption coefficient, leading to the residuals displayed in (d) (blue curve). By smoothing the residuals, the background "continuum" is obtained (green line in (c), also displayed in (a) and (b)).

Considering the signal-to-noise ratio of the analyzed spectrum, the simple method used to derive line intensities and the congestion of the spectrum, we estimate to 10% the error bar to be attached to the line intensities in the most favorable cases. We cannot rule out that a small fraction of weak lines is not real.

The same procedure was applied in the 13 600–13 900 cm^{-1} weaker absorbing region (Fig. 4). In this region, the "continuum" represents most of the absorption, the fitted lines representing no more than 17% of the total absorption. The values of the "continuum" absorption cross-section (in cm^2 per molecule) and the list of the 842 lines fitted in the 13 310–14 000 cm^{-1} are included in the ESI.†

3. Analysis of the CRDS spectrum in the 13 063–13 298 cm^{-1} interval

Cavity ring down spectroscopy (CRDS) with single-frequency CW laser is a highly sensitivity techniques developed in the 90's.[20,21] A noise equivalent absorption as low as $\alpha_{min} \approx 5 \times 10^{-13}$ cm^{-1}, corresponding to a 2% decrease of the transmitted light along an Earth–Moon distance was reported by CRDS in ref. 22. The CRDS technique has been largely applied in the 1.58 μm and 1.28 μm regions of low opacity of methane (transparency windows) both at room temperature and at 80 K.[23–27] In the present work, we took advantage of the availability of a light source near 760 nm at the Institute of Atmospheric Optics in Tomsk to measure methane lines in a region of very low absorption where previous measurements were absent.

3.1. Experimental details and line list construction

An external cavity diode laser (ECDL) from Sacher Lasertechnik, tunable between 13 060 and 13 300 cm^{-1} was used for the recordings. It was initially purchased to characterize with an unprecedented sensitivity the very weak absorption of water vapor interfering with the A-band of oxygen, of particular interest for atmospheric applications.[28,29] The experimental arrangement and data acquisition are similar to those implemented in Grenoble.[22,30] A fiber-optic beam splitter directs 10% of the radiation to a wavelength meter (HighFinesse WS-U, 5 MHz resolution, measurement frequency up to 250 Hz). The remaining 90% is directed to a fiber-optic acousto-optical modulator which interrupts the radiation input into the cavity. At the cavity output, the radiation is focused onto a silicon avalanche photodetector (Thorlabs APD410A) which measures the exponential decay of the intracavity field (ring down time) providing the absolute value of the absorption coefficient.[20,21] The typical ring down time was 180 μs.

The recordings were performed with a pressure of methane of 10 Torr (6670 Pa), measured by a capacitance gauge (50 Torr Inficon CDG020D gauge with 1.0% accuracy of reading). The whole investigated region was covered during two recording sessions (13 060–13 150 cm^{-1} and 13 146–13 300 cm^{-1}) with total duration of about 18 hours. The ring down cell temperature was monitored during the recordings and varied in the 298.1 ± 0.5 K range.

Accurate values of the line positions of O_2 (present as an impurity in the cell) were used to refine the spectral calibration provided by the wavemeter. An RMS of a few 10^{-4} cm^{-1} was achieved for the (meas. − ref.) position differences. We thus estimate our frequency calibration better than 1×10^{-3} cm^{-1}.

An overview of the recorded spectra is included in Fig. 5. The noise equivalent absorption evaluated as the RMS of the noise level is around 3×10^{-11} cm^{-1}, thus about four orders of magnitude lower than that of the above-analyzed KP spectrum.

In view of the extreme spectral congestion revealed by the successive zooms of Fig. 5, the line list construction was performed automatically using the above-described multiline fitting program, the profile of all lines being fixed to a default Voigt profile. At the 10 Torr pressure of the recordings, the pressure broadening is limited to about 8×10^{-4} cm^{-1} (HWHM)[15] and thus the profile is mostly Doppler limited *e.g.* Gaussian with a Doppler HWHM of 2.04×10^{-2} cm^{-1}. The quality of the spectrum reproduction is illustrated by the residuals presented on the lower panel of Fig. 5. The RMS of the

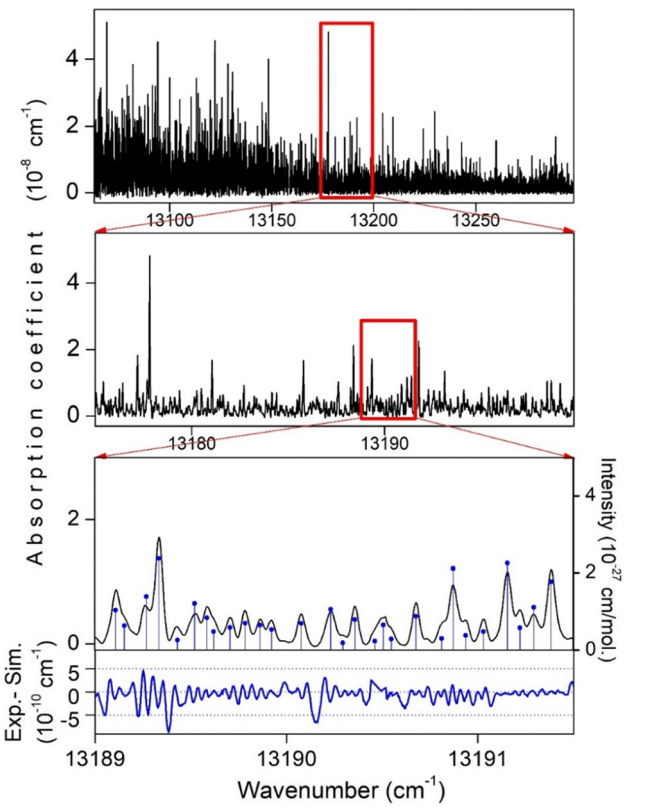

Fig. 5 CRDS spectrum of methane at a pressure of about 10 Torr around 13 200 cm^{-1}. The enlargements illustrate the dynamics achieved on the intensity scale and the noise equivalent absorption ($\alpha_{min} \approx 5 \times 10^{-11}$ cm^{-1}). On the two lower panels, the stick spectrum provided by an automatic multiline fitting procedure is superimposed to the spectrum and the corresponding residuals are displayed. The weakest lines have an intensity of a few 10^{-28} cm per molecule.

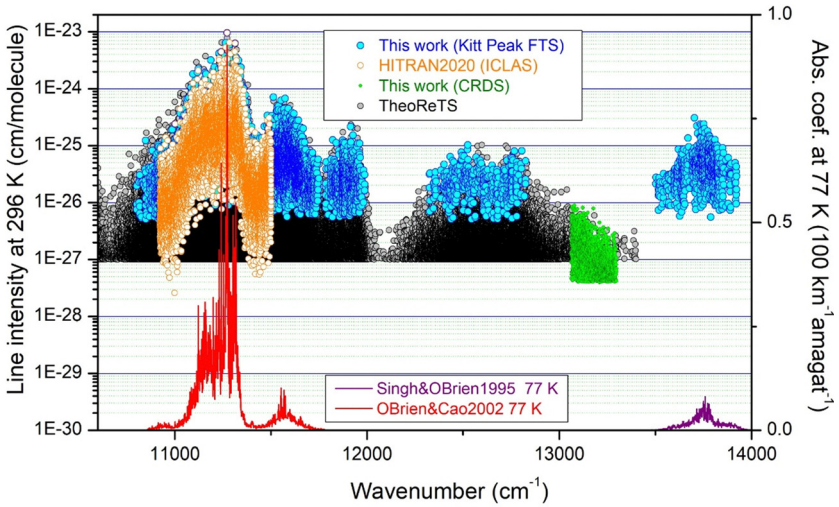

Fig. 6 Overview comparison of the different lines lists of methane available in the 10 500–14 000 cm^{-1} region. The FTS and CRDS line lists retrieved in this work (blue and green circles, respectively) are superimposed to the TheoReTS line list (available up to 13 400 cm^{-1}). The HITRAN line list is also displayed (orange circles). The absorption coefficients at 77 K averaged over 1 cm^{-1} interval are shown in the 10 635–13 300 cm^{-1} and 13 420–14 000 cm^{-1} regions (red and purple curves, respectively). They were measured by ICLAS in ref. 34 and 35, respectively. Note the logarithmic scale used for the line intensities (left hand) while a linear scale is used for the absorption coefficients (right hand).

residuals for the displayed spectral interval is 2×10^{-10} cm^{-1}, thus significantly larger than the experimental noise level.

After a manual removal of the O_2 lines, a total of 1792 methane lines were obtained for the 13 060–13 300 cm^{-1} entire spectral range. It corresponds to a line density of about 10 lines per cm. The weakest lines have an intensity on the order of 5×10^{-28} cm per molecule, about two orders of magnitude lower than the detectivity threshold of the KP spectrum recorded with a ten times larger pressure. Obviously, due to the baseline rough estimation, the intensity of weak lines has a poor accuracy (see residuals in Fig. 5) but for the strongest lines (intensity larger than 5×10^{-27} cm per molecule), we believe that a 5% accuracy is a conservative estimate. The obtained line list is provided as ESI† and included in Fig. 6 where we have gathered the measurements available in the 10 800–14 000 cm^{-1} region that we will discuss in the next section.

3.2. Comparison to the TheoReTS calculated list

We have also included in Fig. 6, the TheoReTS calculated line list[31] computed by Rey *et al.* using variational method using an *ab initio* ACV5Z dipole moment surface.[32] The TheoReTS line list is the most advanced and accurate theoretical methane available to date. This list covers the 0–13 400 cm^{-1} range and is accessible *via* the TheoReTS information system (**https://theorets.univ-reims.fr**, **https://theorets.tsu.ru**). The TheoReTS line list was validated by comparison to Titan spectra as observed by VIMS and by DISR, respectively onboard Cassini and Huygens. It was concluded that TheoReTS is suitable to be used for the modeling of planetary radiative transfer and photometry, in particular because calculations allow for accounting for the unresolved myriads of very weak lines leading to a quasi-continuum.[31]

It is interesting to compare the TheoReTS integrated intensity to the total line intensity measured by CRDS in the 13 063–13 298 cm^{-1} interval. The sum of the experimental intensities (2.69×10^{-24} cm per molecule) represents less than half of the total TheoReTS intensities in the region (5.84×10^{-24} cm per molecule). This disagreement might be due to a quasi-continuum contribution which is not accessible experimentally from the recorded CRDS spectra or to an overestimation of the TheoReTS intensities in the considered region of weak absorption corresponding to the low energy range of the transparency window between the $P = 8$ and $P = 9$ polyads (see Fig. 6). Additional insights on the comparison between the CRDS and TheoReTS intensities in the region are presented below (Section 5) by considering the low resolution methane absorption coefficients recommended in the region by Karkoschka and Tomasko.[33]

4. Review of the literature data and comparison to the KP line list

4.1. Experimental approaches

Our search in the literature indicates that previous laboratory investigations of the high resolution spectrum of methane between 10 800 and 14 000 cm^{-1} are not numerous. This can be partly explained by the weakness of the spectrum which makes necessary to use setups providing sensitivities beyond traditional techniques. Another factor might be the intractable rovibrational interpretation of the spectrum in the considered spectral region. In Table 1, the most relevant previous studies are listed together with our present FTS and CRDS results. The table gives for each source the used experimental techniques, the spectral interval and the temperature conditions. In the last column of the table, some notes indicate the most relevant spectroscopic information provided. The pioneer study by Vedder and Mecke (VM, hereafter) deserves a special mention.[19] In 1933, these authors used photographic plates

Table 1 Review of the most relevant high resolution studies of the $^{12}CH_4$ (and $^{13}CH_4$) absorption spectrum above 10 800 cm^{-1}. The references are grouped according to the experimental technique and for a given technique, they are ordered in increasing energy except for the studies involving jet expansions which are grouped at the end of the table

Spectral range (cm^{-1})	Ref.	Technique[a]	T (K)	Main outputs
9929–13 930	Vedder (1933)[19]	Photographic plates	Room	Above 11 030 cm^{-1}, 366 lines with five intensity grades
10 635–13 300	O'Brien (2002)[34]	ICLAS	Room, 77	77 K abs. coeff. at 77 K averaged over 1 cm^{-1} (or 1 Å) in the 10 859–11 780 cm^{-1} interval
10 923–11 502	HITRAN,[15] Benner (2013)[17]	ICLAS	296	List of 11 200 lines at 296 K extrapolated from low temperature recordings (see Text). Line intensities $>10^{-27}$ cm per molecule. Partial rovibrational assignments
13 787–13 895	Singh (1994)[36]	ICLAS	77, 296	Pressure broadening and shifts by nitrogen, hydrogen, and helium of 4 strong CH_4 lines
13 420–14 000	Singh (1995)[35]	ICLAS	77	13 471–14 024 cm^{-1}: abs. coeff. averaged over 1 cm^{-1} 13 569–13 915 cm^{-1}: 316 lines with abs. coeff. at center
13 420–14 000	Singh (1996)[37]	ICLAS	77	13 471–14 024 cm^{-1}: abs. coeff. averaged over 1 Å
13 777–13 782	Campargue (1989)[42]	ICLAS	Room	
11 170–11 980	Kozlov (2008)[45]	LIGS	Room	*e.g.* Fig. 4 11 480–11 670
11 220–11 930	Kozlov (2013)[46]	LIGS	124–130, 298	Line positions and LIGS relative intensities of about 70 lines
12 720–12 820				Self-broadening and self-shift coefficients for 5 lines
13 720–13 800				
16 100–16 180				
13 530–13 800	Sadovskii (2010)[47]	LIGS	124	Mostly theoretical interpretation
11 200–11 330	Tsukamoto (1995)[48]	TBMS and Stark modulation	77 and 295	269 transitions with relative intensities 215 empirical lower state levels including 49 tetrahedral components.
11 807–11 927	Lucchesini (2007)[49]	WMDLS	294	48 lines with relative peak height
10 802–11 988	This work	FTS	297.7	12 800 lines with intensities $>5\times10^{-27}$ cm per molecule
12 325–12 825				
13 502–13 922				
13 060–13 300	This work	CRDS	300	1792 lines with intensities $>5\times10^{-28}$ cm per molecule
11 170–11 319	Boraas (1995)[50]	$^{13}CH_4$ PAS	100, room	About 500 pos. with rel. int. at 100 K
~11 258	Boraas (1993)[51]	Bolometer, Stark splitting	Jet	Vibrationally induced dipole moment from 3 lines assigned as E symmetry P2, Q2 and R2 of $3\nu_1+\nu_3$
~11 277				
~11 309				
11 220–11 340	Boraas (1994)[52]	Bolometer, PAS Stark splitting	15 (jet), 100, room	About 140 pos. with rel. int. in jet, some low J assignments in particular E symmetry components of P2, Q2 and R2 transitions
11 171–11 315	Campargue (1995)[43]	ICLAS	Jet, room	About 70 positions of low J transitions, 35 rel. int. and a few tentative assignments
13 702–13 887	Campargue (1991)[53]	ICLAS	Jet, room	About 40 positions of low J transitions with relative intensities and a few tentative assignments

[a] Experimental technique: ICLAS: intracavity laser absorption spectroscopy, WMDLS: wavelength modulation diode laser spectroscopy, PAS: photoacoustic spectroscopy, LIGS: laser-induced grating spectroscopy, TBMS: tone-burst modulation spectroscopy.

with exposure times of up to 12 hours, pathlengths of 20 m and pressures up to 5 atm to record the methane spectrum dispersed by a high resolution spectrograph. About 360 line positions were reported between 11 029 and 13 930 cm^{-1}, together with a grade from 0 to 4, increasing with their estimated relative intensities. In the following we will illustrate the good quality of this early list below 12 000 cm^{-1}. At higher energy, its quality degrades.

Except VM data and the present KP spectrum recorded by Fourier transform spectroscopy, all the other experimental approaches are laser-based: ICLAS, wavelength modulation diode laser spectroscopy (WMDLS), photoacoustic spectroscopy (PAS) and laser-induced grating spectroscopy (LIGS).

Most of the previous quantitative measurements were performed in the group of J. O'Brien at the University of Missouri, St. Louis by ICLAS.[34–37] ICLAS is a quantitative technique based on the high sensitivity of a broad-band highly multimode laser to losses induced by a gas absorber placed inside the laser cavity.[38] The broad band laser emission is spectrally dispersed by a high resolution grating spectrograph and time resolved. This technique is quantitative in the sense that it provides absolute absorption coefficients with no need for calibration.[39–41] Indeed, ICLAS is equivalent to classical absorption with an equivalent absorption pathlength, l_{eq}, given by the delay between the beginning of the laser generation and the recording time (called generation time, t_g) multiplied by the light velocity and pondered by the occupation ratio of the laser cavity by the cell (typically 50%). Typical values of the generation time are 100 μs, leading to l_{eq} = 15 km. A noise equivalent absorption $\alpha_{min} \approx 10^{-9}$ cm^{-1} can be achieved allowing for detection of lines with intensity below 10^{-27} cm per molecule.[38] The multimode lasers suitable for ICLAS recordings in the considered region are Ti:sapphire laser[34] and dye lasers,[35,36,42] usually pumped by an argon laser. The ICLAS technique has the advantage to allow for low temperature recordings when combined with a cryogenic cell,[35,36] or with a slit jet gas expansion.[43,44]

The laser-induced grating spectroscopy technique is a highly sensitive non-linear absorption technique which was applied to methane over large spectral ranges.[45–47] The principles of LIGS in molecular gases are presented in.[45,54] Resonant excitation of

molecules in the interference region of two nanosecond pulsed laser beams produces a spatially periodic variation of the population of the energy levels involved. The resulting modulation of the refractive index is detected using a probe beam. In the LIGS recordings of CH_4 spectra reported in ref. 45–47, the pump and probe lasers were dye lasers pumped by a Nd:YAG laser and an argon laser, respectively.

The photoacoustic and wavelength modulation techniques, also used for methane spectroscopy (Table 1), are well known techniques which will not be detailed here. Let us nevertheless mention the tone-burst modulation spectroscopy (TBMS) method[55] implemented by Tsukamoto and Sasada for high sensitivity methane spectroscopy with a Ti:sapphire laser.[48,56] This technique is a type of frequency modulation spectroscopy which relies on the difference between the radiation power transmitted through the absorption cell with and without modulation of the laser radiation. This difference which is phase-sensitively detected provides the methane spectrum.

Regarding the temperature conditions of the recordings, methane has a relatively high saturation pressure of about 10 Torr at liquid nitrogen temperature (77 K) which allows for low temperature recordings of particular interest for planetary applications. The temperature dependence of the methane spectrum at high resolution is considerable (see *e.g.* Fig. 2 of ref. 57 or the movie attached to ref. 58) and a drastic simplification of the spectrum can be achieved by rotational cooling in jet expansions. In our region of interest, this method was applied to methane in the four last studies of Table 1 which will be discussed below.

Let us now consider the methane spectra obtained in the different studies.

4.2. WMDLS between 11 807 and 11 927 cm^{-1} (ref. 49)

Lucchesini *et al.* used wavelength modulation diode laser spectroscopy combined to a multipass Herriott-type cell (L = 30 m) to measure 48 methane lines around 11 850 cm^{-1}. The $\nu_1 + 3\nu_3$ band is predicted to be the dominant band of the region. The line centers were given with a 0.01 cm^{-1} accuracy together with the cross section values at the line centers. Collisional broadening and shift coefficients for different perturbing gases were reported for seven of the most intense lines. The superposition of out KP line list with the WMDLS line list (Fig. 7) indicates that only part of the lines located in the studied interval was measured. Line positions were found generally underestimated from our measurements by up to 1 cm^{-1}. The comparison to the TheoReTS stick spectrum displayed on the lower panel of Fig. 7 illustrates the level of agreement between experiment and theory. A clear correlation is observed for the general appearance of the spectrum and for some of the strongest lines. For these last, the TheoReTS positions deviate by up to 2 cm^{-1}.

4.3 LIGS between 11 807 and 11 927 cm^{-1} (ref. 45–47)

In,[45] the LIGS spectrum of methane was measured between 11 170 and 11 980 cm^{-1} using a narrow-band dye laser Raman-shifted by using a high pressure hydrogen cell. The ambient

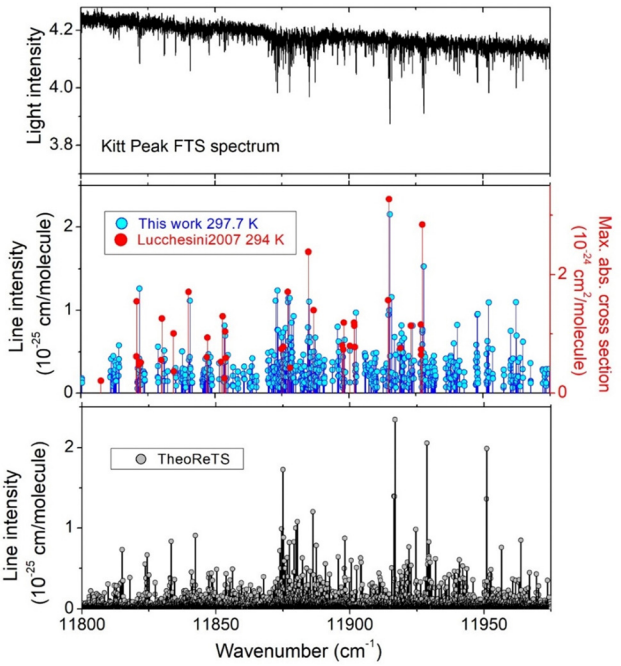

Fig. 7 Overview comparison of the analyzed Kitt Peak spectrum between 10 800 and 11 975 cm^{-1} (upper panel) to the corresponding line list obtained in this work and the WMDLS list reported in ref. 49 (blue and red sticks in the middle panel, respectively) and the TheoReTS line list[31] (lower panel).

temperature spectra were recorded at pressures ranging from 0.2 to 4 bar and minimum values of the cross-sections as low as 10^{-26} cm^2 per molecule were reported. The obtained high resolution spectra were observed to depend strongly on the pressure. According to Fig. 2, 4 and 6 of ref. 45, at the lowest pressure values of the recordings (0.3 and 0.6 bar), the reported LIGS spectra show a similar sensitivity than the above-analyzed KP spectrum. In their following contribution, Kozlov *et al.* extended the LIGS recordings at low temperatures (124–150 K) and higher energies including the regions around 12 700, 13 750 and 16 150 cm^{-1} using different dye lasers.[46] A visual comparison of the LIGS spectrum near 13 750 cm^{-1} (Fig. 7 in ref. 46) to the KP spectrum shows a good agreement and indicates that the LIGS spectrum has a significantly better sensitivity (about one order of magnitude). The situation in the weaker absorbing 12 400–12 900 cm^{-1} region is puzzling. According to Fig. 6 of ref. 46, the LIGS methane spectrum is considerably weaker below than above 12 700 cm^{-1}. This observation is in contradiction with both the KP and ICLAS spectra (see Fig. 6 in ref. 34) and the TheoReTS predictions for which similar absorption extends from 12 500 to 12 900 cm^{-1} (see Fig. 6). We could not find correlation between the KP spectrum and the LIGS spectrum above 12 700 cm^{-1} or the seven lines listed in Table 2 of ref. 46. We thus believe that there was some experimental issue in the LIGS recordings in that particular region. Let us mention that theoretical developments towards the assignment of the high overtone transitions detected by LIGS near 13 750 and 16 150 cm^{-1} were presented in ref. 47. The involved upper vibrational states belong to the

P = 10 and 12 polyads, respectively, for which the traditional normal mode assignment was found questionable at this high level of excitation.

4.4. ICLAS from 10 600 to 13 300 cm^{-1} (ref. 34–37)

The ICLAS technique is a powerful technique which was at the state-of-the-art of high sensitivity absorption techniques in the 90's, before the development of the CRDS technique. The group of Prof. O'Brien devoted important efforts to ICLAS of methane in the 10 600–14 000 cm^{-1} spectral range using Ti:sapphire and dye lasers.[34–37] Absorption path lengths equivalent to several tens km were currently achieved, providing a sensitivity allowing for recordings at low pressure (1–10 Torr). High resolution spectra were recorded with the help of a grating spectrograph dispersing the laser spectrum (resolving power of ~500 000 leading to a width of the apparatus function comparable to the width of the Doppler width of the absorption lines). This spectral resolution allowed for the determination of the pressure-broadening and line-shift coefficients of some methane lines near 727 nm.[36] In addition, the combination with a cryogenic cell allowed for ICLAS of methane at liquid nitrogen temperature (77 K). For all these technical advantages, the ICLAS measurements of methane performed by O'Brien *et al.* remain today at the state-of-the-art in the considered spectral region.

A general overview of the ICLAS recordings can be found in ref. 34. In this reference, the absorption coefficients at 77 K averaged over 1 Å and 1 cm^{-1} intervals are provided for the 10 859–11 780 cm^{-1} region. Similar average values are given in ref. 35 and 37 in the region of the 727 nm band (13 476–14 028 cm^{-1}). For comparison to our line lists, the ICLAS average absorption coefficients are displayed on Fig. 6. To the best of our knowledge, the only ICLAS line list published by O'Brien *et al.* is a peak list at 77 K for the strongest lines between 13 569 and 13 915 cm^{-1} (316 lines in total).[35] The overview comparison of this low temperature list to our KP list at 297 K is presented in Fig. 8. The position agreement is found very good, on the order of a few 10^{-3} cm^{-1} for the strongest lines providing a cross validation of the frequency calibration of the KP and ICLAS spectra (a conservative value of ±0.02 cm^{-1} was attached to the ICLAS position values[35]). As expected, line intensities differ due to the variation of the Boltzmann factor which rules the temperature dependence of the intensities. We tried to combine the ICLAS 77 K peak list and our room temperature KP line list in order to apply the 2T-method[58–61] and derive lower state energy levels, E_{low}, of the transitions in common in the two datasets. Unfortunately, we did not obtain convincing results. The derived E_{low} values did not show a clear propensity to be close to $B_0J(J+1)$ values with $B_0 \approx 5.24$ cm^{-1}. The lack of accuracy of the measured intensity values and the too small number of transitions in common (24) are probably responsible of this failure.

4.5. The region of the $3\nu_1 + \nu_3$ band

The $3\nu_1 + \nu_3$ manifold around 11 280 cm^{-1} corresponding to the strongest absorption above 10 800 cm^{-1} has been the subject of

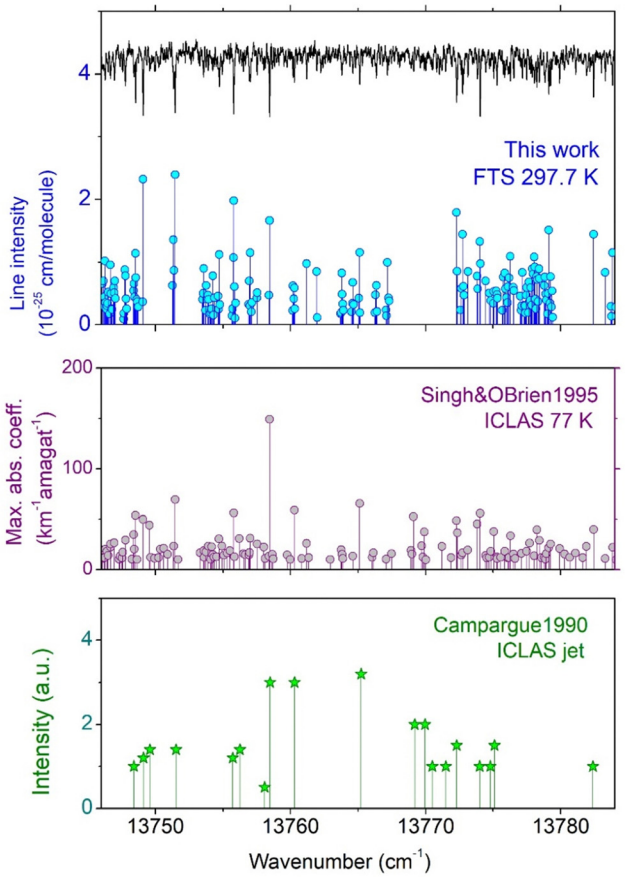

Fig. 8 Overview comparison of the ICLAS peak list at 77 K from[35] (middle panel, purple) to the analyzed Kitt Peak spectrum between 13 740 and 13 790 cm^{-1} and the corresponding KP line list obtained in this work at room temperature (upper panel, blue) and to the peak list obtained by ICLAS of methane rotationally cooled in a slit jet expansion[38] (lower panel, green).

dedicated studies which are presented in this paragraph and in the next one (bulk samples and molecular beam studies, respectively).

4.5(a) ICLAS from 10 923 to 11 502 cm^{-1} included in the HITRAN database[17]. Since its 2012 edition, the HITRAN database provides a line list for methane around 11 250 cm^{-1}.[13] This list relies on ICLAS measurements from O'Brien group (see ref. 34) but unfortunately, the paper[17] quoted as HITRAN source of the HITRAN methane list in the region was not published. Some details on the experimental conditions of the recordings can be found in ref. 13: the ICLAS spectra were recorded at low temperature (99–161 K), low pressure (0.12–7.13 Torr or 16–950 Pa) with equivalent absorption pathlength between 3.14 and 5.65 km and a high spectral resolution (0.01 cm^{-1}). Over 11 200 line positions, intensities and lower state energies, E_{low}, were derived using the multispectrum nonlinear least squares fitting program developed by Benner *et al.*[62]

Let us recall that the resulting HITRAN list (included in Fig. 1 and 6) is given at the HITRAN reference temperature of 296 K. The intensity values at 296 K thus result from an extrapolation of the low temperature ICLAS intensities using the derived empirical E_{low} values. A direct comparison between

the room temperature KP spectrum and a spectrum simulated using the HITRAN line list provides an interesting validation test (Fig. 9). Overall, the agreement is excellent but some significant residuals are nevertheless observed (middle panel of Fig. 9). For instance, a strong line at 11 312.745 cm^{-1} showing a large intensity deviation is highlighted on the lower panel of Fig. 9 (HITRAN and KP intensities at 296 K are 4.47 × 10^{-24} and 1.14 × 10^{-24} cm per molecule, respectively). The comparison to the TBMS results at 77 K presented in Section 4.5(b)[48] confirms that HITRAN intensity value of this line is inaccurate. A rough scaling of the relative intensities reported in ref. 48 (see Fig. 11 below) leads to an HITRAN/TBMS intensity ratio of about 3.0 to be compared to a factor of 3.9 for the HITRAN/KP intensity ratio. Note that the HITRAN lower state, 62.87 cm^{-1} corresponding to J_{low} = 3 agrees with the $R(3)$ assignment reported by Tsukamoto and Sasada, confirming that the temperature extrapolation at 296 K is not responsible of the overestimation of HITRAN intensity value.

Although limited, the deviations between the KP spectrum and the HITRAN simulation motivated us to retrieve the room temperature line parameters from the KP spectrum (see above Section 2). The KP and HITRAN lists are superimposed in Fig. 6. In the 10 923–11 502 cm^{-1} region of the HITRAN list,[17] our list includes 7850 lines while HITRAN list have 11 242 entries. Nevertheless, the sums of the KP and HITRAN line intensities in the region differ by no more than 5% (1.527 × 10^{-21} and 1.448 × 10^{-21} cm per molecule, respectively). Compared to the KP spectrum, the lower pressure of the ICLAS recordings (a few Torr compared to 99.8 Torr) and the lowest temperatures have made possible to resolve a number of blended features which were fitted as single lines in the KP spectrum analysis. In addition, on the edges of the considered region, many weak lines below the detectivity threshold of the KP spectrum were detected by ICLAS. The detection of these weak lines in spectra recorded at much lower pressure illustrates the sensitivity of the ICLAS technique. Note that at low temperature, the line intensity of transitions from low J states is increased by no more than a factor 7 (for J = 0 and a temperature decrease from 296 to 80 K) while for transitions from J > 10 states, the line intensities are decreased by more than two order of magnitude (see Fig. 8 in ref. 63). This could lead to some high J lines missing in the HITRAN list elaborated from low temperature recordings (obviously, hot band transitions are absent). Nevertheless, as recommended line list in the region, we would suggest to correct the HITRAN intensity values of the small number of problematic transitions better than adopting our KP list. Indeed, the higher sensitivity of the ICLAS method and lower pressure of the ICLAS recordings combined with a robust multispectrum treatment of the spectra are supposed to provide better experimental results than the analyzed KP spectrum at about 100 Torr.

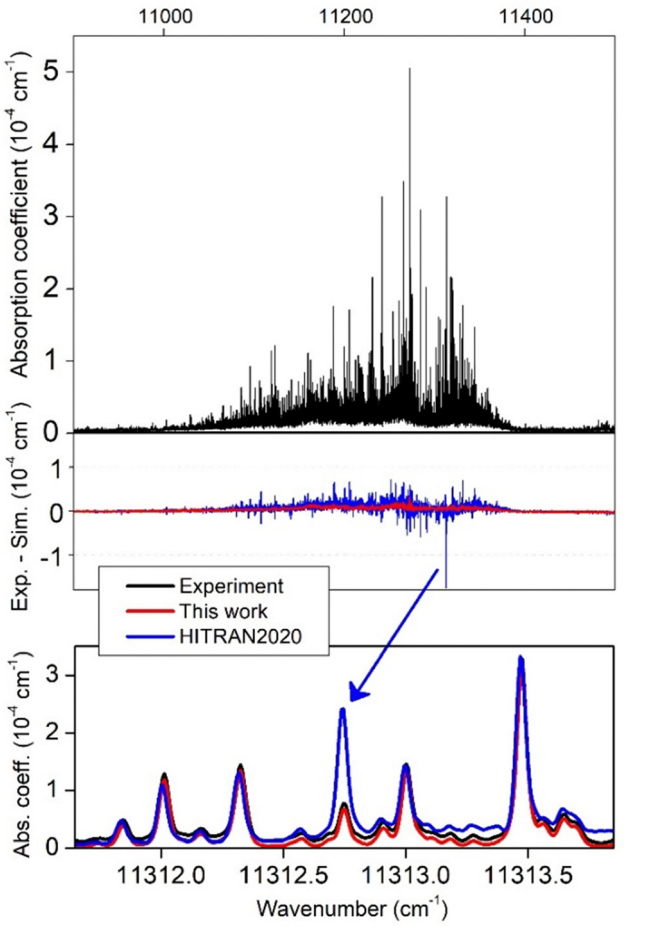

Fig. 9 Upper panel: FTS Kitt Peak spectrum between 10 900 and 11 500 cm^{-1}. Middle panel: Differences between the FTS spectrum and simulations based on the KP line list obtained in this work and the HITRAN line list (red and blue, respectively). Lower panel: Enlargement near 11 313 cm^{-1} showing a line with overestimated HITRAN intensity.[15]

In tribute to the pioneer methane recordings by Vedder and Mecke in the region,[19] we present in Fig. 10, a comparison of their peak list to our KP list and to HITRAN list in the 11 220–11 320 cm^{-1} interval. An obvious coincidence is observed for the strongest lines with position differences limited to a few tenths cm^{-1}. Similar level of agreement is noted for the strongest lines up to 12 000 cm^{-1} but the situation degrades for the ten of lines and the about 70 lines reported near 12 800 and 13 800 cm^{-1}, respectively.

4.5(b) Tone-burst modulation spectroscopy from 11 200 to 11 330 cm^{-1} (ref. 48). In 1995, Tsukamoto and Sasada used a Ti:sapphire laser to perform tone-burst modulation spectroscopy (TBMS) of methane at 77 K and 295 K in the region of the $3\nu_1 + \nu_3$ band. These authors measured 269 transitions at 77 K and 295 K. By applying the 2T-method, they derived empirical lower state energy value and corresponding rotational quantum number, J''. This information combined with Stark modulation spectra at room temperature allowed them to assign 215 of the 269 measured transitions, with respect to J'', of which 49 were identified up to their tetrahedral components. Tsukamoto and Sasada provided relative intensities of the CH_4 lines measured at 77 K. The comparison to the HITRAN line list extrapolated at the same temperature (Fig. 11) shows a very good agreement for line positions (differences of a few 10^{-3} cm^{-1} at most). On Fig. 11, the TBMS relative line intensities were roughly scaled by comparison to HITRAN values. An overall good intensity

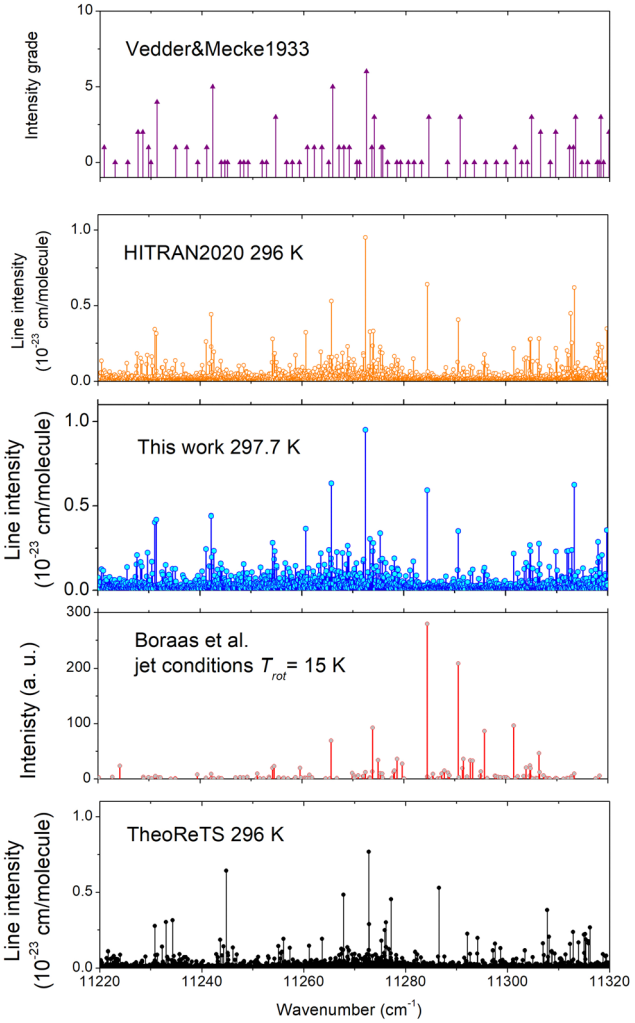

Fig. 10 Comparison of different stick spectra of methane in the region of the $3\nu_1 + \nu_3$ band between 11 220 and 11 320 cm^{-1}. From top to bottom: Vedder and Mecke,[19] HITRAN list at 296 K,[15] FTS line list at 297.7 K derived in this work from the KP spectrum, jet spectrum at a rotational temperature of 15 K reported in ref. 50, TheoReTS line list at 296 K.

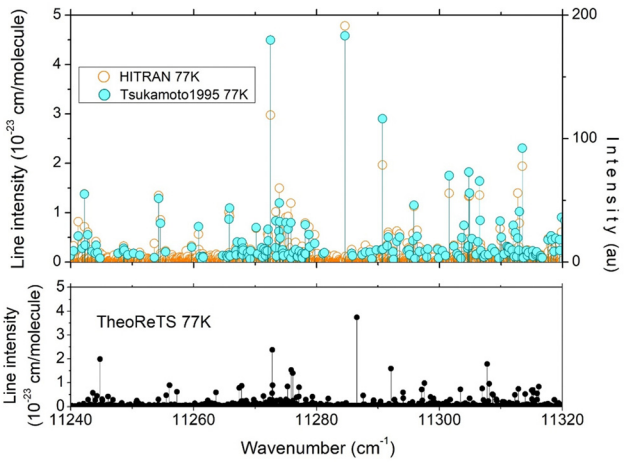

Fig. 11 Comparison of the methane spectrum at 77 K obtained by tone-burst modulation spectroscopy (cyan dots)[48] to the corresponding HITRAN list at 77 K (orange circles)[15] in the region of the $3\nu_1 + \nu_3$ band, between 11 240 and 11 320 cm^{-1}. The corresponding TheoReTS line list at 77 K is displayed on the lower panel.

agreement is achieved. The TBMS intensities show nevertheless a number of deviations by up to 50%. We estimate the detectivity threshold of the TBMS spectrum to be around 2×10^{-25} cm per molecule at 77 K *i.e.* between one and two orders of magnitude above that of the HITRAN and KP lists. We have included the TheoReTS line list at 77 K on the lower panel of Fig. 11. Due to the simplification of the spectrum by rotational cooling, the correspondence between the experimental and TheoReTS transitions is obvious for a few strong lines, significantly easier than at room temperature (Fig. 10). As an example, the strongest line at 11 284.6114 cm^{-1} (2.78×10^{-23} cm per molecule at 77 K) which is assigned as $R(0)$ A1 corresponds to the TheoReTS line at 11 286.572 cm^{-1} (3.74×10^{-23} cm per molecule at 77 K).

4.6. Jet cooled spectroscopy in the 11 170–11 340 cm^{-1} and 13 702–13 887 cm^{-1} regions[43,51–53]

As shown above, rotational cooling is an efficient way to reduce the spectral congestion in order to identify the transitions from the lowest rotational levels. Due to a high saturation pressure at low temperature (a few Torr around 80 K), direct absorption spectroscopy of methane cooled in cryogenic cells has been widely used in the infrared and in the near infrared.[24,57,58,64,65] Above 10 000 cm^{-1}, bulk gas cooling was combined with the above described high sensitivity methods (LIGS, ICLAS, TBMS) but, as a result of the increased spectral congestion, an even more drastic simplification is suitable to help for an interpretation of the spectrum. Rotational temperatures below 20 K can be achieved by using jet expansions. The short pathlength allowed by the jet expansions is a strong limitation for direct absorption, even when slit jets are used. FTS spectroscopy of jet cooled methane is thus mostly limited to the infrared or near infrared.[66–68] Above 10 000 cm^{-1}, to the best of our knowledge, jet-cooled spectroscopy of methane was performed only in the region of the $3\nu_1 + \nu_3$ band around 11 280 cm^{-1} [43,51,52] and in the region of the $4\nu_1 + \nu_3$ band around 13 800 cm^{-1}.[53] Boraas *et al.* used a bolometer to measure the internal energy of jet cooled CH_4 molecules excited by a Ti:sapphire laser downstream a 200 μm diameter nozzle. Campargue *et al.* inserted a slit jet expansion in a dye laser[53] or a Ti:sapphire laser[43] for ICLAS. In order to increase the occupation ratio of the laser cavity by the slit jet expansion, a 24 cm long slit jet was used providing equivalent absorption pathlength of 8 km through the rotationally cooled molecules.[43] The different studies used the temperature dependence of the line intensity to assign the low rotational levels. The level of methane dilution, the nature of the career gas and the stagnation pressure were used to vary the rotational temperature in the gas expansion. In addition, molecular beam Stark spectroscopy was used by Boraas *et al.* to assign the *E*-symmetry components of the $R(2)$, $P(2)$, and $Q(2)$ transitions.[51] It is worth recalling that, due to the conservation of the nuclear spin symmetry in a jet expansion of methane, the relative population corresponding to the (*A*,*E*,*F*) spin symmetry is maintained at very low temperature.[69] As a result, at the low rotational temperature

limit (about 15 K in ref. 52), the population is not concentrated in the $J = 0$ rotational level but distributed to the lowest rotational levels associated with each spin symmetry *i.e.* on the ($J = 0$, A1), ($J = 1$, F1), and ($J = 2$, E) rotational levels, with relative weights corresponding to the room temperature values.[66,69]

Boraas *et al.* measured about 140 line positions between 11 220 and 11 340 cm^{-1} with corresponding relative intensities and provided $J \leq 2$ rotational assignments for about 30 of them on the basis of the temperature dependence and Stark information.[52] The comparison of the line positions to HITRAN values shows an agreement within 0.01 cm^{-1} (see Fig. 10). The rotational assignments were found mostly identical except for a few transitions. For instance, the transition at 11 290.715 cm^{-1} is assigned to $R(0)$ by Boraas *et al.* while HITRAN lower state J value is 2. The $R(0)$ assignment is also that given by Tsukamoto and Sasada by TBMS.[48]

Although only the $3\nu_1 + \nu_3$ band is supposed to bring the intensity in the region, rovibrational coupling to a number of nearby dark states makes the interpretation of the spectrum complicated, even at low temperature.[48] Speculations on the different vibrational bands contributing to the spectrum in the region were presented in.[43,52] Such discussion could now be reconsidered on the basis of the TheoReTS line list in the region (see Fig. 10 and 11).

Regarding the 13 800 cm^{-1} region, a drastic reduction of the spectral congestion was achieved by ICLAS using a 3 cm long slit jet expansion of pure methane with a stagnation pressure of 4 bars and an equivalent absorption path length of 800 m.[53] About 40 positions of low J transitions were reported with relative intensities and ten $J \leq 2$ tentative assignments of three bands were suggested. The ICLAS-jet list is presented in the lower panel of Fig. 8 for comparison to the ICLAS-77K list (middle panel)[35] and KP-296 K list obtained in this work (upper panel). No TheoReTS line list is available in this range and the interpretation of the experimental data available in this region appears to be particularly challenging.

4.7. Minor isotopologues

$^{13}CH_4$. The T_d symmetry being preserved and isotopic shift of the normal mode frequencies being limited to a few wavenumbers, overall, the $^{12}C \rightarrow {}^{13}C$ isotopic substitution of the central carbon atom induces minor changes in the vibrational pattern.[70,71] The $^{13}CH_4$ and $^{12}CH_4$ strong absorption regions thus mostly coincide but, in natural methane, $^{13}CH_4$ bands are typically 100 times weaker as their intensities scale according to the isotopic abundance factor (1.1%). In absence of recordings performed with $^{13}CH_4$ enriched sample, $^{13}CH_4$ lines are included in the retrieved empirical line lists but remain unidentified.

In the 10 800–14 000 cm^{-1} region under consideration, experimental data relative to $^{13}CH_4$ are limited to two studies: (i) about 300 $^{13}CH_4$ lines identified in the HITRAN list between 11 170 and 11 320 cm^{-1}.[17] As mentioned above, the paper describing the origin of the HITRAN list in this region remains unpublished and we do not know how the $^{13}CH_4$ lines were identified in the ICLAS spectra of natural methane, (ii) Boraas *et al.* dedicated a specific study to the $^{13}CH_4$ isotopologue in the region of the $3\nu_1 + \nu_3$ band around 11 280 cm^{-1}.[50] Photoacoustic spectra of $^{13}CH_4$ were recorded at 100 K and 293 K and a peak list of 561 lines was constructed from the 100 K spectrum. This list might have been used to identify $^{13}CH_4$ transitions in the ICLAS line list of natural methane provided in the HITRAN database. The $3\nu_1 + \nu_3$ band of $^{13}CH_4$ was observed shifted with respect to that of the $^{12}CH_4$ isotopologue by 30.55 cm^{-1} but the rotational structure is completely different.[50]

We have examined the Kitt Peak archives and did not find FTS spectra of the $^{13}CH_4$ isotopologue in our region of interest. The TheoReTS line list of $^{13}CH_4$ has been calculated in a similar way as for the main isotopologue and is available up to 13 400 cm^{-1}.[31]

Deuterated methane. The substitution of one or several hydrogen atoms by deuterium leads to drastic changes in some vibrational frequencies and a change of the symmetry group (C_{3v} for CH_3D and CHD_3, C_{2v} for CH_2D_2). As a result, although the strongest bands remain those involving the CH stretching mode, the absorption spectrum of deuterated methane shows important differences compared to those of the CH_4 species.

CH_3D. In spite of a relative abundance limited to 5×10^{-4}, the knowledge of the methyl deuteride spectrum is relevant for planetary applications as the CH_3D detection may give access to the D/H abundance ratio. Due to important isotopic shifts, strong CH_3D bands may be located in CH_4 transparency windows. In the region of these CH_3D bands, the CH_3D relative contribution to the methane absorption is much higher than the CH_3D isotopic abundance and may even dominate in some specific spectral intervals (see for instance[63,65,72] for a discussion of the importance of the CH_3D absorption in the 1.58 μm methane transparency window). This planetary interest has motivated pioneer works in our region starting with the recordings using photographic plates obtained by Bardwell and Herzberg.[73] Using a 1 atm pressure of CH_3D and an 88 m absorption pathlength, these authors estimated eight band centers in our region dominated by the $\Delta V_{CH} = 4$ and $\Delta V_{CH} = 5$ bands near 11 280 and 13 753 cm^{-1}. In 1977, using the same method but with a higher resolution spectrograph, Danehy *et al.* resolved the J rotational structure of the band centered at 11 931.13 cm^{-1} (and of two other bands below our region, at 9389.9 and 10 405 cm^{-1}).[74] Later, intracavity photoacoustic spectroscopy at 100 K allowed to resolve and partly assign the K-subband structure of this band which shows a mostly regular appearance.[75] In their work, Lin *et al.* reported measured line positions for the band centered at 11 931.13 cm^{-1} and mentioned three other bands at 11 019, 11 181 and 11 288 cm^{-1} with highly congested rotational structure. We note some similarity in the general appearance of the $\Delta V_{CH} = 4$ bands in CH_3D and CH_4: the most excited $\Delta V_{CH} = 4$ band, namely $\nu_1 + 3\nu_3$ near 11 880 cm^{-1} for CH_4 (Fig. 7), appears to be the most isolated (*i.e.* the least perturbed).

A general overview of the medium resolution absorption spectrum of CH_3D in the 11 000–11 500 cm^{-1} and 13 500–14 000 cm^{-1} intervals can be found in.[76] The spectrum in the former interval was recorded by FTS with a pressure of 298 Torr and a path length of 7 m. The spectra in the latter interval corresponding to $\Delta V_{CH} = 5$ bands were recorded by phase shift

cavity ring down at 297 and 125 K. Although the spectral resolution was insufficient to extract line list, integrated cross-sections were determined in the two regions.[76]

In summary, high resolution data of CH_3D in our region are mostly limited to the 11 931 cm^{-1} band analyzed in.[75] As it mostly coincides with the $\nu_1 + 3\nu_3$ band of CH_4 near 11 880 cm^{-1}, this band is not particularly favorable to be used for CH_3D detection in planetary spectra.

CH_2D_2. To the best of our knowledge, no high resolution experimental data are available for the CH_2D_2 isotopologue in our region of interest. The most relevant data are low resolution spectra in the region of the $\Delta V_{CH} = 5$ manifold (13 300–14 300 cm^{-1}) recorded by photoacoustic spectroscopy at room temperature[77] and phase shift cavity ring down at 297 and 125 K.[76] The strongest peak near 13 784 cm^{-1} is accompanied by a few combination bands which were tentatively assigned.

CHD_3. In spite of its limited interest for atmospheric applications, the visible spectrum of the CHD_3 isotopologue has been extensively studied up to 18 500 cm^{-1}, in particular in our laboratory.[78–85] The main reason of these extended investigations is related to the fact that the dominant bands of this C_{3v} symmetric top isotopologue are regular up to a high energy and show a well resolved rotational structure which can be easily assigned. This matter of fact is related to the single CH bond which makes the CH stretching mode isolated from the other vibrational modes except for a strong coupling with the ν_b CHD bending mode.[81] The latter having a frequency of about half that of the CH stretching frequency, the coupling between vibrational states with the same $N = \nu_s + \nu_b/2$ polyad number is very efficient and the oscillator strength brought by the CH stretching mode is redistributed over the vibrational states with the same N value. As a result of this anharmonic interaction, a series of $2N + 1$ bands is observed for each N value. Vibrational bands with upper states in the N = 3.5, 4 and 4.5 polyads fall in the 10 800–14 000 cm^{-1} region. They have been extensively studied by FTS[81] and by ICLAS,[83,84] leading to interesting studies of the dynamics and intramolecular vibrational relaxation processes.[81,86–88]

5. Low resolution simulations, comparison to band models

As mentioned in the introduction, the knowledge of methane absorption spectrum is necessary to analyse planetary data in particular to evaluate the heat balance in the atmospheres of the outer planets and Titan. At high energies, in absence of line lists of methane transitions with known temperature dependence of their intensities, astronomers have adopted a pragmatic approach and use an empirical modelling of low resolution methane spectra.[33,89,90] Karkoschka and Tomasko (KT hereafter) have combined datasets from eight laboratory measurements recorded in a large variety of temperature conditions and measurements from space (Titan's atmosphere spectrum by the Huygens probe, Jupiter spectrum by the Hubble Space Telescope) to provide reliable methane absorption coefficients in the wide 1800–25 000 cm^{-1} range at three temperatures (100, 198 and 296 K).[33] Bowles *et al.* derived methane absorption coefficients and the modelling of their T dependence in the 9000–14 000 cm^{-1} range on the basis of a series of FTS spectra measured at the Rutherford Appleton Laboratory (UK) over a wide range of pressures (38 mbar to 5 bar), temperatures (100–298 K) and path lengths (14.4–19.3 m).[90] The spectra were recorded at a medium resolution of 0.12 cm^{-1} and then averaged to 10 cm^{-1}.

For comparison purpose to the KT and Bowles absorption coefficients, low resolution spectra were simulated using the FTS and CRDS line lists obtained in this work and using the TheoReTS calculated line list. Absorption coefficients at 296 K (in km^{-1} $amagat^{-1}$ = 3.25 × 10^{-25} cm per molecule) were obtained by convolution of the line lists by a Gaussian "apparatus function" with full-width at half medium of 5 cm^{-1}. The overview of the comparison is presented in Fig. 12. For the present experimental data, we have displayed both the simulations limited to the lines and the sum of the line and "continuum" absorption. At the logarithmic scale of the plot, the overall agreement appears to be satisfactory but several observations deserve to be mentioned: (i) in the high energy region, above 12 000 cm^{-1}, our FTS line list represents only a small fraction of the methane absorption, probably due to both the insufficient sensitivity of the analysed KP spectrum and the importance of the unresolved background continuum (ii) in the region around 13 800 cm^{-1}, by adding the (dominant) contribution of the experimentally determined "continuum" to the line absorption, the total absorption is found in very good agreement with both KT and TheoReTs absorption coefficients, (iii) the absorption coefficients reported by Bowles *et al.* appear to be significantly overestimated over the whole spectral range. The overestimation is on the order of 50% near 11 200 cm^{-1} but

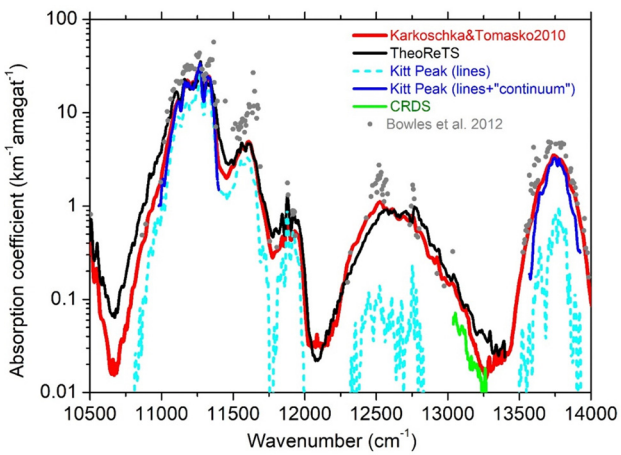

Fig. 12 Comparison of the methane absorption coefficients obtained by Karkoschka and Tomasko[33] (red line) and Bowles *et al.*[90] (grey dots) to low resolution simulations obtained from the $^{12}CH_4$ TheoReTS line list (black), from the line list retrieved from the present analysis of the Kitt Peak FTS spectrum of natural methane (dashed cyan) and from the present CRDS list of natural methane near 13 200 cm^{-1}. Around 11 200 and 13 800 cm^{-1}, an absorption "continuum" was retrieved from the Kitt Peak spectrum and added to the absorption of the lines leading to the total absorption (solid blue).

increases up to 100% near 11 600 cm^{-1}. A similar observation was noted in the 9028–10 435 cm^{-1} range.[16]

In Fig. 13, we compare in more details low resolution simulations in the absorption region of the $3\nu_1 + \nu_3$ band around 11 220 cm^{-1}. In this region, the "continuum" absorption retrieved from the KP spectrum represents about half of the lines absorption (lower panel of Fig. 13). The obtained total KP absorption nicely agrees with KT absorption coefficients. It seems that TheoReTS absorption is overestimated in the low and high energy edges of the displayed absorption region (where KT and KP absorptions coincide). On the lower panel of Fig. 13, a low resolution simulation based on the HITRAN list is superimposed and found in good agreement with the KP absorption limited to the lines. Thus the HITRAN list does not account for the "continuum" part of the absorption in this region. This is understandable because, as explained above, the HITRAN line list is the result of an extrapolation at 296 K of line lists retrieved from low temperature ICLAS spectra.[13,17] At least, part of the "continuum" is due to the superposition of weak lines from high J levels or hot bands which are not observed at low temperature but show up at 296 K. Another possible reason is that the derivation of continua from ICLAS spectra is challenging as the baseline of the ICLAS spectra is usually only a few tens cm^{-1} wide with a shape fixed by the broad band multimode laser emission (a Ti:sapphire in the present case).[38]

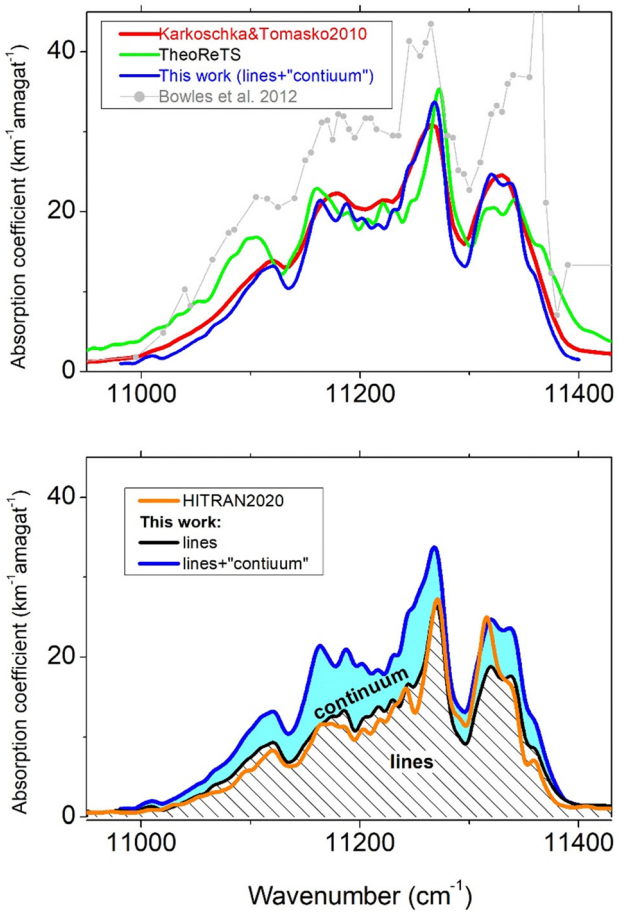

Fig. 13 Comparison of low resolution methane absorption coefficients near 11 220 cm^{-1} corresponding to the region of the $3\nu_1 + \nu_3$ band. On the upper panel, absorption coefficients by Karkoschka and Tomasko[33] (red line) and Bowles *et al.*[90] (grey dots) are compared to low resolution simulations obtained from the $^{12}CH_4$ TheoReTS line list[31] (black) and from the analysis of the Kitt Peak FTS spectrum of natural methane (blue). The latter includes both the absorption of the lines and the absorption "continuum" which are separated on the lower panel (dashed pattern and cyan background, respectively). The low resolution simulation obtained using the HITRAN2020 list of methane is also included on the lower panel (solid orange line).

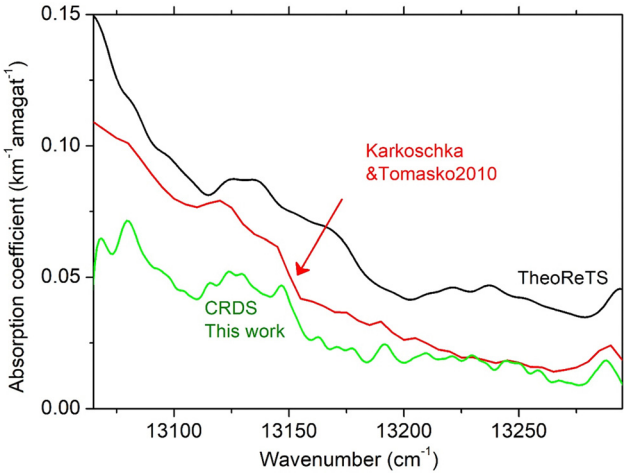

Fig. 14 Comparison of low resolution methane absorption coefficients near 13 200 cm^{-1}: absorption coefficients by Karkoschka and Tomasko[33] (red line) are compared to low resolution simulations obtained from the $^{12}CH_4$ TheoReTS line list[31] (black) and from the line list retrieved in this work from CRDS spectra between 13 063 and 13 298 cm^{-1}.

The TheoReTS absorption seems to be also overestimated in the region of very low absorption measured by CRDS around 13 250 cm^{-1} (Fig. 14). A possible impact of the "continuum" has to be ruled out as in principle, the "continuum" is included in the KT absorption coefficients. On the contrary, around 13 100 cm^{-1}, the CRDS absorption is about half the KT and TheoReTS absorptions. The "continuum" which could not be evaluated from our CRDS measurements might be responsible of this missing absorption. Let us recall that the CRDS and KT methane absorptions include the contribution of all the isotopologues while the considered TheoReTS list is limited to $^{12}CH_4$.

6. Conclusion and perspectives

As mentioned in the introduction, the complexity of the methane spectrum in the visible range results from strong rovibrational interactions within vibrational polyads whose size dramatically increases with energy. The overview presented in Fig. 15 indicates that the presently considered 10 800–14 000 cm^{-1} region corresponds to the P = 8–10 polyads (namely pentacontakaipentad, heptacontad and enneacontakaihenad, involving 996, 1746 and 2954 sublevels, respectively[13]). The vibrational mixing at this high energy is such that the normal mode labeling of the vibrational

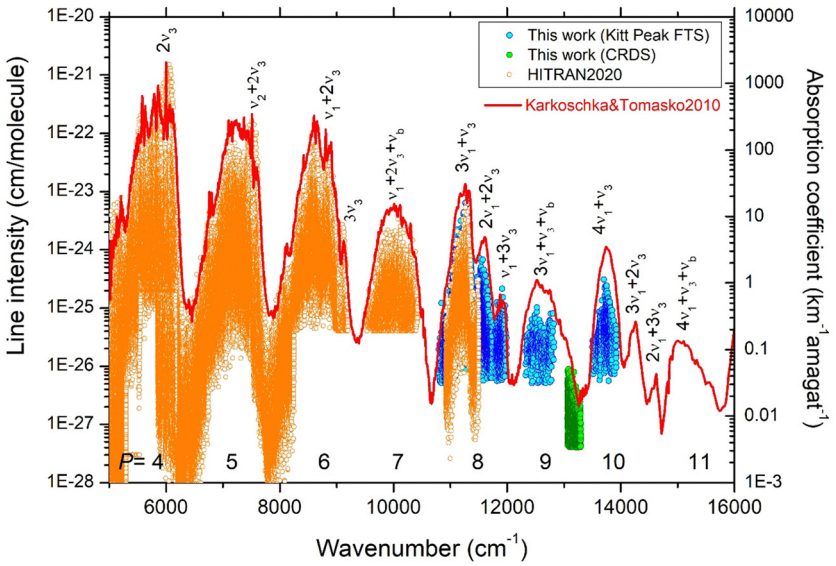

Fig. 15 The methane absorption in the 5000–16 000 cm^{-1} region. Overview comparison of the absorption coefficients by Karkoschka and Tomasko[33] (red line) to the HITRAN line list (orange circles) and the line lists obtained in this work: Kitt Peak FTS data and CRDS data (blue and green dots, respectively). The polyad number $P = 2(V_1 + V_3) + V_2 + V_4$ is indicated together with the most probable assignment of the dominant band (ν_b stands for both bending modes, ν_2 and ν_4).

bands should be used with much caution.[47] Nevertheless, as a rule, in each polyad, the dominant bands are expected to correspond to upper vibrational states involving the maximum stretching excitation (bright states). Due to a difference of about 100 cm^{-1} of the ν_1 and ν_3 stretching frequencies (2916 and 3019 cm^{-1}, respectively), at high energy, the energy separation between the different stretching bands of a given polyad increases, reducing the overlapping of their rotational structure. Consequently, their unperturbed rotational structure may be partly preserved. For instance, the $3\nu_3$ band at the high energy range of the $P = 6$ polyad near 9046 cm^{-1}, shows a PQR rotational structure very similar to that of the ν_3 fundamental band.[16,91] In our spectral region, the absorption associated to the three purely stretching bands of the $P = 8$ polyad – $3\nu_1 + \nu_3$, $2\nu_1 + 2\nu_3$ and $\nu_1 + 3\nu_3$ – can be easily located near 11 280, 11 550 and 11 880 cm^{-1} (Fig. 15). As reviewed above, the region of the $3\nu_1 + \nu_3$ band corresponding to the strongest band system region has been studied using different experimental approaches (see Table 1): ICLAS, TBMS, PAS at room and low temperature, Stark spectroscopy, rotational cooling in molecular beam. As a result, this band system is the only one for which a significant number of transitions has been rotationally assigned[17,48,52] but the identification of the different vibrational bands contributing to the spectrum remains an open issue.

In the case of the $\nu_1 + 3\nu_3$ band presented in Fig. 7, the general appearance of the TheoReTS predictions seems in better agreement with the observations than in the region of the $3\nu_1 + \nu_3$ band (Fig. 10 and 11). In particular, the positions and intensities of the strongest lines at 11 915.2909 and 1197.906 cm^{-1} are in relatively good coincidence with TheoReTS counterparts at 11 916.7887 and 11 928.7212 cm^{-1}, respectively, (position differences on the order of 1.4 cm^{-1}). The lower state energy value provided in the TheoReTS line list allows us to propose a $R(2)$ and $R(3)$ assignment for these two transitions, respectively. Such examples of rovibrational assignments by direct comparison to the TheoReTS list are extremely scarce. The systematic rovibrational assignment of the experimental lists based on TheoReTS predictions supplemented by effective Hamiltonian modeling was performed up to the icosad ($P = 5$)[14] but seems presently out of reach in our region. An additional difficulty in the case of the CH_4 molecule is the limited possibility to use lower state combination difference relations to validate and propagate rovibrational assignments.

The completeness of the theoretical line lists which inherently include the temperature dependence of the calculated intensity is a unique advantage for application to low resolution spectra or radiative transfer calculations but, the present accuracy of state-of-the-art theoretical calculations is not sufficient for applications to the analysis of spectra of exoplanetary atmospheres at high spectral resolution. In terms of transition frequencies, theoretical methods do not reach experimental accuracy. In our region, the TheoReTS list transition frequencies can deviate from observations by up to a few cm^{-1}. Below 8000 cm^{-1}, the deviations were found to be mostly dependent on the vibrational bands with limited rotational dependence (see *e.g.* ref. 14). In the TheoReTS $^{12}CH_4$ list (available at **https://theorets.univ-reims.fr** or **https://theorets.tsu.ru**), part of the line positions (up to the icosad region near 7800 cm^{-1}) have experimental accuracies as, when possible, TheoReTS variational transition frequencies were empirically corrected according to available experimental data.

The ExoMol line list of methane[92] was not considered for the above comparisons because its quality is significantly lower than the TheoReTS list. The ExoMol and TheoReTS lists rely on different potential energy surfaces and dipole moment surfaces obtained from advanced *ab initio* electronic structure

calculations. The ExoMol list is provided up to 12 000 cm^{-1} but its quality degrades sharply in this region. As illustrated in Fig. 16, the absorption corresponding to the $3\nu_1 + \nu_3$ manifold near 11 280 cm^{-1} has its ExoMol maximum shifted to lower energy by about 120 cm^{-1} and the strongest ExoMol lines have an intensity about four times larger than the measured and TheoReTS values.

Thus, the experimental approach appears to be the only way to obtain line lists with sufficient line position accuracy to fulfil future needs for the detection of methane from high resolution exoplanetary atmospheres spectra in the visible range. The above review of the experimental works in the 10 800–14 000 cm^{-1} region has pointed some deficiencies of our present knowledge. Above 11 500 cm^{-1}, no extensive line lists were systematically retrieved from the high resolution spectra obtained by ICLAS and LIGS. Only absorption coefficients at 77 K averaged over 1 cm^{-1} in the 10 859–11 780 cm^{-1} and 13 471–14 024 cm^{-1} intervals and a peak list of 316 lines at 77 K between 13 569 and 13 915 cm^{-1} were obtained from ICLAS spectra[34,35] – see Table 1 and Fig. 6. In this context, our room temperature KP line list above 11 500 cm^{-1} constitutes a first step towards the construction of a high resolution line list of methane in the visible range.

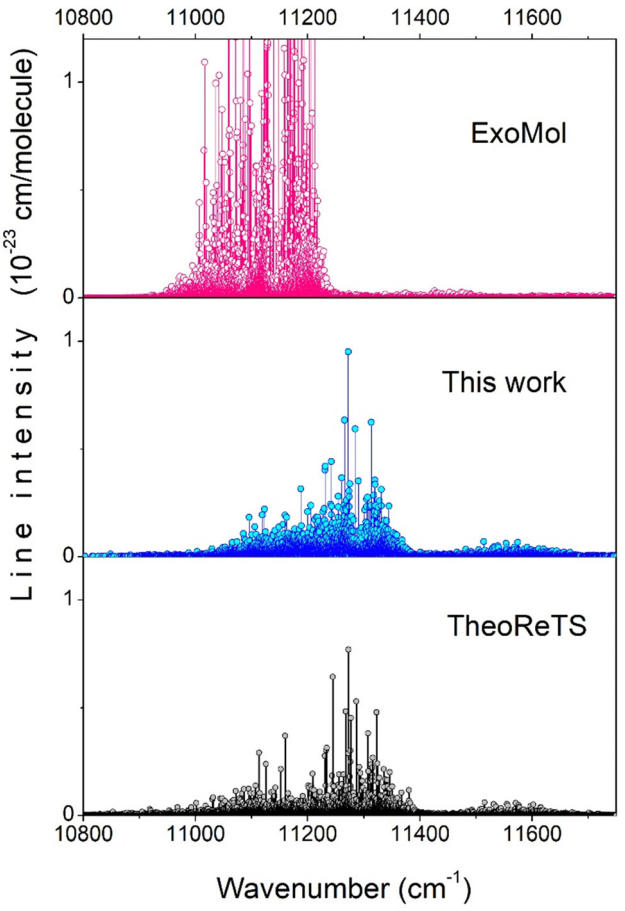

Fig. 16 Comparison of the ExoMol[92] and TheoReTS[31] calculated line lists to the KP experimental line list obtained in this work between 10 800 and 11 750 cm^{-1}.

The high sensitivity LIGS recordings at 130 K and 300 K were not exploited to construct line lists. Only line positions of 71 prominent features measured between 11 230 and 16 170 cm^{-1} were reported with relative intensities and a 0.01 cm^{-1} position accuracy.[46] Being a non-linear technique, the LIGS method is not optimum for quantitative intensity measurements as illustrated by the unexpected variation of the LIGS line intensities in the 12 400–12 800 cm^{-1} region (see Section 4.3). Let us nevertheless mention that the LIGS spectrum at 124 K displayed in Fig. 7 of ref. 46 for the 13 730–13 800 cm^{-1} region and the ICLAS peak list at 77 K of ref. 35 show a good agreement both for line positions and relative line intensities and seem to have comparable sensitivity (better than that of the KP spectrum analyzed in this work – see Fig. 8)

In this work, the analysis of FTS and CRDS spectra have provided new data above 11 500 cm^{-1} where extensive line lists were missing but further improvements are both suitable and achievable. The present CRDS study at room temperature in the 13 063–13 298 cm^{-1} interval shows that the routine sensitivity of modern CRDS setups allow for measurements with a detectivity threshold below 10^{-27} cm per molecule, the main limitation in the data treatment being the spectral congestion and not the signal-to-noise of the spectra (see Fig. 5). All the lines presently measured by CRDS are below the sensitivity of the presently analyzed KP spectrum recorded by FTS. In principle, the spectral coverage of the Ti:sapphire laser allows for CRDS recordings over the entire 10 800–14 000 cm^{-1} spectral region but tuning such a laser over a more than 3000 cm^{-1} wide spectral region is extremely laborious. Alternatively, a series of diode lasers (in particular external cavity diode lasers as used in the present CRDS recordings) could be used in some more limited spectral intervals. An alternative would be the mode-lock cavity enhanced technique which is another cavity-enhanced method providing quantitative measurements at high sensitivity.[93,94] As for ICLAS, the dispersion of the spectrum can be performed using a high resolution spectrograph and spectra are acquired using a ccd array which provides the multiplex advantage and reduces the acquisition time. The recent development of dual comb spectroscopy and Vernier spectroscopy has opened new possibilities for rapid acquisition of high resolution spectra in the near infrared. Broadband high-resolution molecular spectra undistorted by the instrumental line shape can be recorded with a highly precise frequency scale provided by the frequency comb.[95,96] Optical frequency comb Fourier transform spectroscopy has been applied to the high accuracy absorption measurements of CH_4 transitions in the 1250–1380 cm^{-1} interval[97] while dual-comb spectroscopy was used in the region of the ν_3 band near 3.4 μm,[98] of the $2\nu_3$ band near 1.6 μm[99] and in the icosad region (6770–7570 cm^{-1}) at high temperature.[100] In our region of interest where the methane absorption is weak, cavity-enhanced absorption is suitable to achieve a sufficient sensitivity. Several high sensitivity cavity-enhanced measurements have been reported by dual-comb spectroscopy mostly in the telecom region (*e.g.* ref. 95 and 101). A mode-locked Ti:sapphire laser has been used for cavity-enhanced frequency comb vernier spectroscopy in our

region.[102] The Vernier continuous filtering technique combining an optical frequency comb with a high finesse cavity allows for measurement of the full optical frequency comb spectrum with high sensitivity, GHz resolution and sub-second acquisition time[103] (see ref. 104 for a recent review of this method). This technique seems particularly suitable for methane spectroscopy in the region as illustrated by the quality of the broadband high resolution spectrum of the A band of oxygen reported over the large 12 200–13 200 cm^{-1} region.[105]

In addition to accurate line positions and intensities, a requirement for high resolution exoplanetary applications is the knowledge of the temperature dependence of the line intensities. This requirement is highly demanding for experiment. Indeed, in absence of rovibrational assignments, the temperature dependence of the line intensities can be determined using the 2T-method which supposes the availability of spectra at two temperatures (or more) in order to empirically determine the lower state energy of the transitions from the temperature variation of their line intensities. Recordings at low temperature providing a large temperature gap are possible in the case of methane (see for instance the ICLAS recordings at 77 K in ref. 35 and 36, PAS at 100 K in ref. 50 and 52, LIGS at 130 K in ref. 46 – see Table 1) but the combination of a cryogenic cells for high resolution cavity-enhanced spectroscopy is very demanding.[24]

Although of limited impact for high resolution applications, an interesting result obtained from the analysis of the KP spectrum is the quantitative evaluation of an underlying quasi continuum at room temperature in the regions near 11 200 and 13 800 cm^{-1} (Fig. 3 and 4, respectively). In the 11 200 cm^{-1} region, on the basis of spectra simulations at pressure of the KP spectrum (99.8 Torr) using the HITRAN list and default pressure broadening coefficient of 0.0750 cm^{-1} atm^{-1}, we checked that the evidenced continuum is not due to a cumulative effect of intermediate or far wings of the pressure broadened lines. [Note that in the visible range, methane line profiles are not affected by intramolecular vibrational energy relaxation (IVR)[106].] This is confirmed both by (i) the close agreement between the sum of the KP and HITRAN line intensities and (ii) the close agreement between the ''lines + continuum'' absorption and the low resolution absorption coefficients proposed by Karkoschka and Tomasko.[33] In the 10 772–11 457 cm^{-1} region, the ''continuum'' representing about 30% of the total absorption must thus be added to the (HITRAN or KP) absorption of the lines to account for the methane absorption at room temperature. The relative importance of the ''continuum'' is larger in the 13 800 cm^{-1} region and is expected to increase with the energy.

These ''continua'' are believed to be the result of the cumulative effect of numerous weak lines which are too dense to be resolved and measured. Photoacoustic spectra of methane with Doppler limited resolution were recorded at 77 K, 195 K and room temperature near 16 115 cm^{-1} in.[106] While at room temperature, the spectrum appears as mostly unresolved and structureless, clear absorption lines show up at low temperature. The partitioning of the methane absorption in a contribution corresponding to lines with intermediate or large intensities and a quasi-continuum formed by the weak lines was proposed in.[107,108] For an efficient simulation of billions of calculated weak lines which are necessary for the modeling of the methane absorption at high temperature, the concept of ''super-lines'' was introduced.[108] Experimentally, this approach was applied to FTS hot methane absorption spectra at 1200 K in the infrared region[109] and empirical line list and quasi-continuum cross sections were provided in a similar way as adopted in the present work in the 11 200 and 13 800 cm^{-1} regions.

The search of methane in exoplanetary atmospheres using new methods such as spectral correlation has renewed the interest of high resolution spectroscopic data of methane above 10 000 cm^{-1}. In the present work, we have provided a detailed line list at room temperature of CH_4 covering the 10 800–14 000 cm^{-1} (0.71–0.93 μm) region, with a typical line position uncertainty of 5×10^{-3} cm^{-1} and a line intensity threshold of 5×10^{-27} cm per molecule. The KP line list provided as a ESI† includes the first extensive list of methane transitions above 11 500 cm^{-1}. It will be used to interpret reflected light observations of Titan already obtained with VLT@ESPRESSO in ultra-high spectral resolution mode, with $R = \lambda/\Delta\lambda = \sigma/\Delta\sigma$ = 180 000 (run 106.218L.001, PI: M. Turbet). The line list can now be used to build empirical masks to search for methane in the atmosphere of exoplanets, using visible light high-resolution ground-based spectrographs.

However, the quality of the reported KP line list is limited by the sensitivity of the FTS technique. The above review of the literature has indicated that most of the previous studies are several decades old and do not provide quantitative intensity information at high spectral resolution. We thus suggest to revisit the methane spectrum above 11 500 cm^{-1} by applying modern cavity-enhanced techniques as was done in the present work by CRDS over the 13 060–13 300 cm^{-1} small interval. The obtained data will not only fulfil needs for planetary applications but also provide robust dataset for future theoretical analysis of the spectrum of this important molecule.

Conflicts of interest

There are no conflicts to declare.

Acknowledgements

We acknowledge funding from the Agence Nationale de la Recherche (e_PYTHEAS ANR-16-CE31-0005 and ANR-RNF TEMMEX-ANR-21-3 0 CE-0053-01). This work is supported by CNRS (France) in the frame of the International Research Project ''SAMIA''. SV (Tomsk) acknowledges the support by the Ministry of Science and High Education of the Russian Federation (Project No. FWRU-2021-0006). MT thanks the Gruber Foundation for its support to this research. MT acknowledges support from the Tremplin 2022 program of the Faculty of Science and Engineering of Sorbonne University.

References

1 F. Pepe, S. Cristiani, R. Rebolo, N. C. Santos, H. Dekker, A. Cabral, P. Di Marcantonio, P. Figueira, G. Lo Curto, C. Lovis, M. Mayor, D. Mégevand, P. Molaro, M. Riva, M. R. Zapatero Osorio, M. Amate, A. Manescau, L. Pasquini, F. M. Zerbi, V. Adibekyan, M. Abreu, M. Affolter, Y. Alibert, M. Aliverti, R. Allart, C. Allende Prieto, D. Álvarez, D. Alves, G. Avila, V. Baldini, T. Bandy, S. C. C. Barros, W. Benz, A. Bianco, F. Borsa, V. Bourrier, F. Bouchy, C. Broeg, G. Calderone, R. Cirami, J. Coelho, P. Conconi, I. Coretti, C. Cumani, G. Cupani, V. D'Odorico, M. Damasso, S. Deiries, B. Delabre, O. D. S. Demangeon, X. Dumusque, D. Ehrenreich, J. P. Faria, A. Fragoso, L. Genolet, M. Genoni, R. Génova Santos, J. I. González Hernández, I. Hughes, O. Iwert, F. Kerber, J. Knudstrup, M. Landoni, B. Lavie, J. Lillo-Box, J. L. Lizon, C. Maire, C. J. A. P. Martins, A. Mehner, G. Micela, A. Modigliani, M. A. Monteiro, M. J. P. F. G. Monteiro, M. Moschetti, M. T. Murphy, N. Nunes, L. Oggioni, A. Oliveira, M. Oshagh, E. Pallé, G. Pariani, E. Poretti, J. L. Rasilla, J. Rebordão, E. M. Redaelli, S. Santana Tschudi, P. Santin, P. Santos, D. Ségransan, T. M. Schmidt, A. Segovia, D. Sosnowska, A. Sozzetti, S. G. Sousa, P. Spanò, A. Suárez Mascareño, H. Tabernero, F. Tenegi, S. Udry and A. Zanutta, ESPRESSO at VLT on-sky performance and first results, *J. Astron. Astrophys.*, 2021, **645**, A96, DOI: **10.1051/0004-6361/202038306**.

2 C. Lovis, N. Blind, B. Chazelas, J. G. Kühn, L. Genolet, I. Hughes, M. Sordet, R. Schnell, M. Turbet, T. Fusco, J. F. Sauvage, M. Bugatti, N. Billot, J. Hagelberg, E. Hocini and O. Guyon RISTRETTO: high-resolution spectroscopy at the diffraction limit of the VLT. Society of Photo-Optical Instrumentation Engineers (SPIE) Conference Series 2022; **12184**:121841Q, DOI: **10.1117/12.2627923**.

3 A. Marconi, M. Abreu, V. Adibekyan, V. Alberti, S. Albrecht, J. Alcaniz, M. Aliverti, C. Allende Prieto, J. D. Alvarado Gómez, P. J. Amado, M. Amate, M. I. Andersen, E. Artigau, C. Baker, V. Baldini, A. Balestra, S. A. Barnes, F. Baron, S. C. C. Barros, S. M. Bauer, M. Beaulieu, O. Bellido-Tirado, B. Benneke, T. Bensby, E. A. Bergin, K. Biazzo, A. Bik, J. L. Birkby, N. Blind, I. Boisse, E. Bolmont, M. Bonaglia, X. Bonfils, F. Borsa, A. Brandeker, W. Brandner, C. H. Broeg, M. Brogi, D. Brousseau, A. Brucalassi, J. Brynnel, L. A. Buchhave, D. F. Buscher, A. Cabral, G. Calderone, R. Calvo-Ortega, B. L. Canto Martins, F. Cantalloube, L. Carbonaro, G. Chauvin, B. Chazelas, A. L. Cheffot, Y. S. Cheng, A. Chiavassa, L. Christensen, R. Cirami, N. J. Cook, R. J. Cooke, I. Coretti, S. Covino, N. Cowan, G. Cresci, S. Cristiani, V. Cunha Parro, G. Cupani, V. D'Odorico, I. de Castro Leão, A. De Cia, J. R. De Medeiros, F. Debras, M. Debus, O. Demangeon, M. Dessauges-Zavadsky, P. Di Marcantonio, F. Dionies, R. Doyon, J. Dunn, D. Ehrenreich, J. P. Faria, C. Feruglio, M. Fisher, A. Fontana, M. Fumagalli, T. Fusco, J. Fynbo, O. Gabella, W. Gaessler, E. Gallo, X. Gao, L. Genolet, M. Genoni, P. Giacobbe, E. Giro, R. S. Gonçalves, O. Gonzalez, J. I. González Hernández, F. Gracia Témich, M. G. Haehnelt, C. Haniff, A. Hatzes, R. Helled, H. J. Hoeijmakers, P. Huke, S. Järvinen, A. Järvinen, A. Kaminski, A. Korn, D. Kouach, G. Kowzan, L. Kreidberg, M. Landoni, A. Lanotte, A. Lavail, J. Li, J. Liske, C. Lovis, S. Lucatello, D. Lunney, M. MacIntosh, N. Madhusudhan, L. Magrini, R. Maiolino, L. Malo, A. Man, T. Marquart, E. L. Marques, A. M. Martins, C. J. A. P. Martins, P. Maslowski, C. Mason, E. Mason, R. A. McCracken, P. Mergo, G. Micela, T. Mitchell, P. Mollière, M. Monteiro, D. Montgomery, C. Mordasini, J. Morin, A. Mucciarelli, M. T. Murphy, M. N'Diaye, B. Neichel, A. T. Niedzielski, E. Niemczura, L. Nortmann, P. Noterdaeme, N. Nunes, L. Oggioni, E. Oliva, H. Önel, L. Origlia, G. Östlin, E. Palle, P. Papaderos, G. Pariani, J. Peñate Castro, F. Pepe, L. Perreault Levasseur, P. Petit, L. Pino, J. Piqueras, A. Pollo, K. Poppenhaeger, A. Quirrenbach, E. Rauscher, R. Rebolo, E. M. A. Redaelli, S. Reffert, D. T. Reid, A. Reiners, P. Richter, M. Riva, S. Rivoire, C. Rodríguez-López, I. U. Roederer, D. Romano, S. Rousseau, J. Rowe, S. Salvadori, N. Santos, P. Santos Diaz, J. Sanz-Forcada, M. Sarajlic, J. F. Sauvage, S. Schäfer, R. P. Schiavon, T. M. Schmidt, C. Selmi, S. Sivanandam, M. Sordet, R. Sordo, F. Sortino, D. Sosnowska, S. G. Sousa, E. Stempels, K. G. Strassmeier, A. Suárez Mascareño, A. Sulich, X. Sun, N. R. Tanvir, F. Tenegi-Sanginés, S. Thibault, S. J. Thompson, A. Tozzi, M. Turbet, P. Vallée, R. Varas, K. Venn, J. P. Véran, A. Verma, M. Viel, G. Wade, C. Waring, M. Weber, J. Weder, B. Wehbe, J. Weingrill, M. Woche, M. Xompero, E. Zackrisson, A. Zanutta, M. R. Zapatero Osorio, M. Zechmeister and J. Zimara ANDES, the high resolution spectrograph for the ELT: science case, baseline design and path to construction. Society of Photo-Optical Instrumentation Engineers (SPIE) Conference Series 2022; 12184:1218424, DOI: **10.1117/12.2628689**.

4 R. Allart, L. Pino, C. Lovis, S. G. Sousa, N. Casasayas-Barris, M. R. Zapatero Osorio, M. Cretignier, E. Palle, F. Pepe, S. Cristiani, R. Rebolo, N. C. Santos, F. Borsa, V. Bourrier, O. D. S. Demangeon, D. Ehrenreich, B. Lavie, M. Lendl, J. Lillo-Box, G. Micela, M. Oshagh, A. Sozzetti, H. Tabernero, V. Adibekyan, C. Allende Prieto, Y. Alibert, M. Amate, W. Benz, F. Bouchy, A. Cabral, H. Dekker, V. D'Odorico, P. Di Marcantonio, X. Dumusque, P. Figueira, R. Genova Santos, J. I. González Hernández, G. Lo Curto, A. Manescau, C. J. A. P. Martins, D. Mégevand, A. Mehner, P. Molaro, N. J. Nunes, E. Poretti, M. Riva, A. Suárez Mascareño, S. Udry and F. Zerbi, WASP-127b: a misaligned planet with a partly cloudy atmosphere and tenuous sodium signature seen by ESPRESSO, *J. Astron. Astrophys.*, 2020, **644**, A155, DOI: **10.1051/0004-6361/202039234**.

5 M. Lafarga, M. Brogi, S. Gandhi, H. M. Cegla, J. V. Seidel, L. Doyle, R. Allart, N. Buchschacher, M. Lendl, C. Lovis and D. Sosnowska, The hot Neptune WASP-166 b with ESPRESSO – III. A blue-shifted tentative water signal constrains the presence of clouds, *J. Mon. Not. Royal Astron. Soc.*, 2023, **521**(1), 1233–1252, DOI: **10.1093/mnras/stad480**.

6 I. A. G. Snellen, R. J. de Kok, E. J. W. de Mooij and S. Albrecht, The orbital motion, absolute mass and high-altitude winds of exoplanet HD 209458b, *Nature*, 2010, **465**, 1049–1051, DOI: 10.1038/nature09111.
7 P. Mollière and I. A. G. Snellen, *Astron. Astrophys.*, 2019, **622**, A139, DOI: 10.1051/0004-6361/201834169.
8 M. Brogi and J. Birkby, ExoFrontiers; Big Questions in Exoplanetary, *Science*, 2021, 8, DOI: 10.1088/2514-3433/abfa8fch8.
9 C. Lovis, I. Snellen, D. Mouillet, F. Pepe, F. Wildi, N. Astudillo-Defru, J. L. Beuzit, X. Bonfils, A. Cheetham, U. Conod, X. Delfosse, D. Ehrenreich, P. Figueira, T. Forveille, J. H. C. Martins, S. P. Quanz, N. C. Santos, H. M. Schmid, D. Ségransan and S. Udry, Atmospheric characterization of Proxima b by coupling the SPHERE high-contrast imager to the ESPRESSO spectrograph, *J. Astron. Astrophys.*, 2017, **599**, A16, DOI: 10.1051/0004-6361/201629682.
10 M. Leung, V. S. Meadows and Y. Lustig, High-resolution spectral discriminants of ocean loss for M-dwarf terrestrial exoplanets, *Astron. J.*, 2020, **160**(1), 11, DOI: 10.3847/1538-3881/ab9012.
11 C. Sagan, W. R. Thompson, R. Carlson, D. Gurnett and C. Hord, A search for life on Earth from the Galileo spacecraft, *Nature*, 1993, **365**(6448), 715–721, DOI: 10.1038/365715a0.
12 E. W. Schwieterman, N. Y. Kiang, M. N. Parenteau, C. E. Harman, S. DasSarma, T. M. Fisher, G. N. Arney, H. E. Hartnett, C. T. Reinhard, S. L. Olson, V. S. Meadows, C. S. Cockell, S. I. Walker, J. L. Grenfell, S. Hegde, S. Rugheimer, R. Hu and T. W. Lyons, Exoplanet Biosignatures: A Review of Remotely Detectable Signs of Life, *Astrobiology*, 2018, **18**(6), 663–708, DOI: 10.1089/ast.2017.1729.
13 L. R. Brown, K. Sung, D. C. Benner, V. M. Devi, V. Boudon and T. Gabard, *et al.*, Methane line parameters in the HITRAN2012 database, *J. Quant. Spectrosc. Radiat. Transfer*, 2013, **130**, 201–219, DOI: 10.1016/j.jqsrt.2013.06.020.
14 M. Rey, A. V. Nikitin, A. Campargue, S. Kassi, D. Mondelain and V. G. Tyuterev, *Ab initio* variational predictions for understanding highly congested spectra: rovibrational assignment of 108 new methane sub-bands in the icosad range (6280–7800 cm^{-1}), *Phys. Chem. Chem. Phys.*, 2016, **18**, 176–189, DOI: 10.1039/C5CP05265C.
15 I. E. Gordon, L. S. Rothman, R. J. Hargreaves, R. Hashemi and E. V. Karlovets, *et al.*, The HITRAN2020 molecular spectroscopic database, *J. Quant. Spectrosc. Radiat. Transfer*, 2021, 107949, DOI: 10.1016/j.jqsrt.2021.107949.
16 S. Béguier, A. W. Liu and A. Campargue, An empirical line list for methane near 1 μm (9028–10,435 cm^{-1}), *J. Quant. Spectrosc. Radiat. Transfer*, 2015, **166**, 6–12, DOI: 10.1016/j.jqsrt.2015.07.003.
17 D. C. Benner, V. M. Devi, J. J. O'Brien, S. Shaji, P. T. Spickler, C. P. Houck, J. A. Coakley, J. Dolph and K. Rankin, Empirical line parameters of CH_4 from 10 923 to 11 502 cm^{-1}, unpublished.
18 D. M. Dennison and S. B. Ingram, A new band in the absorption spectrum of methane gas, *Phys. Rev.*, 1930, **36**(9), 1451, DOI: 10.1103/PhysRev.36.1451.
19 H. Vedder and R. Mecke, Das Rotationsschwingungsspektrum des Methans, *Z. Med. Phys.*, 1933, **86**, 137–156, DOI: 10.1007/BF01343281.
20 D. Romanini, A. A. Kachanov, N. Sadeghi and F. Stoeckel, CW cavity ring down spectroscopy, *Chem. Phys. Lett.*, 1997, **264**, 316–322, DOI: 10.1016/S0009-2614(96)01351-6.
21 D. Romanini, I. Ventrillard, G. Méjean, J. Morville and E. Kerstel, Introduction to Cavity Enhanced Absorption Spectroscopy, *Springer Series in Optical Sciences*, 2014, vol. 179, pp. 1–60, DOI: 10.1007/978-3-642-40003-2-1.
22 S. Kassi and A. Campargue, Cavity ring down spectroscopy with 5×10^{-13} cm^{-1} sensitivity, *J. Chem. Phys.*, 2012, **137**(23), 234201, DOI: 10.1063/1.4769974.
23 A. W. Liu, S. Kassi and A. Campargue, High sensitivity CW-cavity ring down spectroscopy of CH_4 in the 1.55 μm transparency window, *Chem. Phys. Lett.*, 2007, **447**, 16–20, DOI: 10.1016/j.cplett.2007.08.092.
24 S. Kassi, D. Romanini and A. Campargue, Mode by Mode CW-CRDS at 80 K: Application to the 1.58 μm transparency window of CH_4, *Chem. Phys. Lett.*, 2009, **477**(1–3), 17–21, DOI: 10.1016/j.cplett.2009.06.097.
25 A. Campargue, L. Wang, A. W. Liu, S. M. Hu and S. Kassi, Empirical line parameters of methane in the 1.63-1.48 μm transparency window by high sensitivity Cavity Ring Down Spectroscopy, *J. Chem. Phys.*, 2010, **373**(3), 203–210, DOI: 10.1016/j.chemphys.2010.05.011.
26 D. Mondelain, S. Kassi, L. Wang and A. Campargue, The 1.28 μm transparency window of methane (7541–7919 cm^{-1}): empirical line list and temperature dependence (80 K–300 K), *Phys. Chem. Chem. Phys.*, 2011, **13**(17), 7985–7996, DOI: 10.1039/c0cp02948c.
27 C. De Bergh, R. Courtin, B. Bézard, A. Coustenis, E. Lellouch, M. Hirtzig, P. Rannou, P. Drossart, A. Campargue, S. Kassi, L. Wang, V. Boudon, A. Nikitin and V. Tyuterev, Applications of a new set of methane line parameters to the modeling of Titan's spectrum in the 1.58 μm window, *J. Planet Space Sci.*, 2012, **61**(1), 85–99, DOI: 10.1016/j.pss.2011.05.003.
28 S. Vasilchenko, S. N. Mikhailenko and A. Campargue, Water vapor absorption in the region of the oxygen A-band near 760 nm, *J. Quant. Spectrosc. Radiat. Transfer*, 2021, **275**, 107847, DOI: 10.1016/j.jqsrt.2021.107c.
29 S. Vasilchenko, S. N. Mikhailenko and A. Campargue, Cavity ring down spectroscopy of water vapour near 750 nm: a test of the HITRAN2020 and W2020 line lists, *J. Mol. Phys.*, 2022, **120**(15–16), e2051762, DOI: 10.1080/00268976.2022.2051762.
30 P. Macko, D. Romanini, S. N. Mikhailenko, O. V. Naumenko, S. Kassi, A. Jenouvrier, V. Tyuterev and A. Campargue, High sensitivity CW-cavity ring down spectroscopy of water in the region of the 1.5 μm atmospheric window, *J. Mol. Spectrosc.*, 2004, **227**, 90–108, DOI: 10.1016/j.jms.2004.05.020.
31 M. Rey, A. V. Nikitin, B. Bézard, P. Rannou, A. Coustenis and V. G. Tyuterev, New accurate theoretical line lists of $^{12}CH_4$ and $^{13}CH_4$ in the 0–13 400 cm^{-1} range: Application to the modeling of methane absorption in Titan's atmosphere, *Icarus*, 2018, **303**, 114–130. https://theorets.univ-reims.fr or https://theorets.tsu.ru.

32 A. V. Nikitin, M. Rey and V. G. Tyuterev, Accurate line intensities of methane from first-principles calculations, *J. Quant. Spectrosc. Radiat. Transfer*, 2017, **200**, 90–99, DOI: 10.1016/j.jqsrt.2017.05.023.
33 E. Karkoschka and M. Tomasko, Methane absorption coefficients for the Jovian planets from laboratory, Huygens and HST data, *Icarus*, 2010, **205**(2), 674–694, DOI: 10.1016/j.icarus.2009.07.044.
34 J. J. O'Brien and H. Cao, Absorption spectra and absorption coefficients for methane in the 750–940 nm region obtained by intracavity laser spectroscopy, *J. Quant. Spectrosc. Radiat. Transfer*, 2002, **75**(3), 323–350, DOI: 10.1016/S0022-4073(02)00015-8.
35 K. Singh and J. J. O'Brien, Laboratory measurements of absorption coefficients for the 727 nm band of methane at 77 K and comparison with results derived from spectra of the giant planets, *J. Quant. Spectrosc. Radiat. Transfer*, 1995, **54**(4), 607–619, DOI: 10.1016/0022-4073(95)00102-Q.
36 K. Singh and J. J. O'Brien, Measurement of pressure-broadening and lineshift coefficients at 77 and 296 K of methane lines in the 727 nm band using intracavity laser spectroscopy, *J. Quant. Spectrosc. Radiat. Transfer*, 1994, **52**(1), 75–87, DOI: 10.1016/0022-4073(94)90140-6.
37 K. Singh and J. J. O'Brien, Absorption coficients for the 727 nm band of methane at 77 K determined by intracavity laser spectroscopy, *Astrophys. Space Sci.*, 1996, **236**, 97–109, DOI: 10.1007/BF00644324.
38 A. Campargue, F. Stoeckel and M. Chenevier, High sensitive intracavity laser spectroscopy: Applications to the study of overtone transitions in the visible range, *Spectrochim. Acta Rev.*, 1990, **13**(1), 69–88.
39 M. Chenevier, M. A. Melieres and F. Stoeckel, Intracavity absorption line shapes and quantitative measurements on O_2, *Opt. Commun.*, 1983, **45**(6), 385–391, DOI: 10.1016/0030-4018(83)90296-1.
40 M. A. Mélières, M. Chenevier and F. Stoeckel, Intensity measurements and self-broadening coefficients in the γ band of O_2 at 628 nm using intracavity laser-absorption spectroscopy (ICLAS), *J. Quant. Spectrosc. Radiat. Transfer*, 1985, **33**, 337–345, DOI: 10.1016/0022-4073(85)90195-5.
41 B. Kalmar and J. J. O'Brien, Quantitative Intracavity Laser Spectroscopy Measurements with a Ti:sapphire Laser: Absorption Intensities for Water Vapor Lines in the 790–800 nm Region, *J. Mol. Spectrosc.*, 1998, **192**(2), 386–393, DOI: 10.1006/jmsp.1998.7705.
42 A. Campargue, M. Chenevier and F. Stoeckel, High-resolution overtone spectroscopy of SiH_4 and $SiHD_3$ (Δv_{SiH} = 6) and CH_4 (Δv_{CH} = 5), *J. Chem. Phys.*, 1989, **138**(2–3), 405–411, DOI: 10.1016/0301-0104(89)87146-0.
43 A. Campargue, D. Permogorov and R. Jost, Intracavity absorption spectroscopy of the third stretching overtone transition of jet cooled methane, *J. Chem. Phys.*, 1995, **102**, 5910–5916, DOI: 10.1063/1.469325.
44 A. Campargue, L. Biennier, A. Kachanov, R. Jost, B. Bussery-Honvault, V. Veyret, S. Churassy and R. Bacis, Rotationally resolved absorption spectrum of the O_2 dimer in the visible range, *Chem. Phys. Lett.*, 1998, **288**, 734–742, DOI: 10.1016/S0009-2614(98)00294-2.
45 D. N. Kozlov and P. P. Radi, Detection of vibrational overtone excitation in methane by laser-induced grating spectroscopy, *J. Raman Spectrosc.*, 2008, **39**(6), 730–738, DOI: 10.1002/jrs.1928.
46 D. N. Kozlov, D. A. Sadovski and P. P. Radi, Laser-induced grating spectroscopy of highly excited overtone and combination vibrational states of methane, *J. Mol. Spectrosc.*, 2013, **291**, 23–32, DOI: 10.1016/j.jms.2013.04.005.
47 D. A. Sadovskii, D. N. Kozlov and P. P. Radi, Direct absorption transitions to highly excited polyads 8, 10, and 12 of methane, *Phys. Rev. A: At., Mol., Opt. Phys.*, 2010, **82**(1), 012503, DOI: 10.1103/PhysRevA.82.012503.
48 T. Tsukamoto and H. Sasada, Extended assignments of the $3\nu_1 + \nu_3$ band of methane, *J. Chem. Phys.*, 1995, **102**, 5126–5140, DOI: 10.1063/1.469238.
49 A. Lucchesini and S. Gozzini, Methane diode laser overtone spectroscopy at 840 nm, *J. Quant. Spectrosc. Radiat. Transfer*, 2007, **103**(1), 209–216, DOI: 10.1016/j.jqsrt.2006.02.056.
50 K. Boraas and J. P. Reilly, The $3\nu_1 + \nu_3$ vibrational overtone spectrum of $^{13}CH_4$, *J. Chem. Phys.*, 1995, **190**(2–3), 301–309, DOI: 10.1016/0301-0104(94)00314-Z.
51 K. Boraas, D. F. De Boer, Z. Lin and J. P. Reilly, The Stark effect in methane's $3\nu_1 + \nu_3$ vibrational overtone band, *J. Chem. Phys.*, 1993, **99**, 1429–1432, DOI: 10.1063/1.465388.
52 K. Boraas, Z. Lin and J. P. Reilly, High resolution study of methane's $3\nu_1 + \nu_3$ vibrational overtone band, *J. Chem. Phys.*, 1994, **100**, 7916–7927, DOI: 10.1063/1.466837.
53 A. Campargue, M. Chenevier and F. Stoeckel, Intracavity-laser-absorption spectroscopy of the visible overtone transition of methane in a supersonically cooled jet, *Chem. Phys. Lett.*, 1991, **183**(1–2), 153–157, DOI: 10.1016/0009-2614(91)85116-E.
54 H. J. Eichler, P. Günter and D. W. Pohl, *Laser-Induced Dynamic Gratings*, Springer, Berlin, 1986, DOI: 10.1007/978-3-540-39662-8.
55 H. M. Pickett, Determination of collisional linewidths and shifts by a convolution method, *Appl. Opt.*, 1980, **19**(16), 2745–2749, DOI: 10.1364/AO.19.002745.
56 H. Sasada, T. Tsukamoto, Y. Kuba, N. Tanaka and K. Uehara, *J. Opt. Soc. Am. B*, 1994, **11**, 191.
57 L. Wang, S. Kassi and A. Campargue, Temperature dependence of the absorption spectrum of CH_4 in the region of the $2\nu_3$ band at 1.66 μm by absorption spectroscopy at 81 K, *J. Quant. Spectrosc. Radiat. Transfer*, 2010, **111**, 1130, DOI: 10.1016/j.jqsrt.2009.10.019.
58 S. Kassi, B. Gao, D. Romanini and A. Campargue, The near-infrared (1.30–1.70 μm) absorption spectrum of methane down to 77 K, *Phys. Chem. Chem. Phys.*, 2008, **10**, 4410–4419, DOI: 10.1039/B805947K.
59 A. Campargue, L. Wang, S. Kassi, M. Mašát and O. Votava, Temperature dependence of the absorption spectrum of CH_4 by high resolution spectroscopy at 81 K: (II) The Icosad region (1.49–1.30 μm), *J. Quant. Spectrosc. Radiat. Transfer*, 2010, **111**(9), 1141–1151, DOI: 10.1016/j.jqsrt.2009.11.025.

60 E. Sciamma-O'Brien, S. Kassi, B. Gao and A. Campargue, Experimental low energy values of CH_4 transitions near 1.33μm by absorption spectroscopy at 81K, *J. Quant. Spectrosc. Radiat. Transfer*, 2009, **110**(12), 951–963.

61 L. Wang, D. Mondelain, S. Kassi and A. Campargue, The absorption spectrum of methane at 80 and 294 K in the icosad (6717–7589 cm^{-1}): Improved empirical line lists, isotopologue identification and temperature dependence, *J. Quant. Spectrosc. Radiat. Transfer*, 2012, **113**(1), 47–57, DOI: **10.1016/j.jqsrt.2011.09.003**.

62 D. C. Benner, C. P. Rinsland, V. M. Devi, M. A. H. Smith and D. Atkins, A multispectrum non linear least squares fitting technique, *J. Quant. Spectrosc. Radiat. Transfer*, 1995, **53**, 705–721, DOI: **10.1016/0022-4073(95)00015-D**.

63 A. Campargue, L. Wang, D. Mondelain, S. Kassi, B. Bézard, E. Lellouch, A. Coustenis, C. Bergh, M. Hirtzig and P. Drossart, An empirical line list for methane in the 1.26–1.71 μm region for planetary investigations (T = 80–300 K): application to Titan, *Icarus*, 2012, **219**, 110–128, DOI: **10.1016/j.icarus.2012.02.015**.

64 J. S. Margolis, Empirical values of the ground state energies for methane transitions between 5500 and 6150 cm^{-1}, *J. Appl. Opt.*, 1990, **29**, 2295–2302, DOI: **10.1364/AO.29.002295**.

65 L. Wang, S. Kassi, A. W. Liu, S. M. Hu and A. Campargue, High sensitivity absorption spectroscopy of methane at 80 K in the 1.58 μm transparency window: Temperature dependence and importance of the CH_3D contribution, *J. Mol. Spectrosc.*, 2010, **261**(1), 41–52, DOI: **10.1016/j.jms.2010.02.005**.

66 A. Amrein, M. Quack and U. Schmitt, High-resolution interferometric Fourier transform infrared absorption spectroscopy in supersonic free jet expansions: carbon monoxide, nitric oxide, methane, ethyne, propyne, and trifluoromethane, *J. Phys. Chem.*, 1988, **92**(19), 5455–5466, DOI: **10.1021/j100330a025**.

67 R. Georges, M. Herman, J. C. Hilico and O. Robert, High-Resolution FTIR Spectroscopy Using a Jet: Sampling the Rovibrational Spectrum of $^{12}CH_4$, *J. Mol. Spectrosc.*, 1998, **187**(1), 13–20, DOI: **10.1006/jmsp.1997.7462**.

68 M. Herman, R. Georges, M. Hepp and D. Hurtmans, High resolution Fourier transform spectroscopy of jet-cooled molecules, *Int. Rev. Phys. Chem.*, 2000, **19**(2), 277–325, DOI: **10.1080/01442350050020905**.

69 M. Hepp, G. Winnewisser and K. M. T. Yamada, Conservation of the nuclear spin modification of CH_4 in the cooling process by supersonic jet expansion, *J. Mol. Spectrosc.*, 1994, **164**(1), 311–314, DOI: **10.1006/jmsp.1994.1074**.

70 M. Rey, A. V. Nikitin and Vl. G. Tyuterev, Predictions for methane spectra from potential energy and dipole moment surfaces: Isotopic shifts and comparative study of $^{13}CH_4$ and $^{12}CH_4$, *J. Mol. Spec.*, 2013, **291**, 85–97, DOI: **10.1016/j.jms.2013.04.003**.

71 O. N. Ulenikov, E. S. Bekhtereva, S. Albert, S. Bauerecker, H. M. Niederer and M. Quack, Survey of the high resolution infrared spectrum of methane ($^{12}CH_4$ and $^{13}CH_4$): Partial vibrational assignment extended towards 12 000 cm^{-1}, *J. Chem. Phys.*, 2014, **141**, 234302, DOI: **10.1063/1.4899263**.

72 Y. Lu, D. Mondelain, S. Kassi and A. Campargue, The CH_3D absorption spectrum in the 1.58 μm transparency window of methane: Empirical line lists and temperature dependence between 80 K and 296 K, *J. Quant. Spectrosc. Radiat. Transfer*, 2011, **112**, 2683–2697, DOI: **10.1016/j.jqsrt.2011.07.009**.

73 J. Bardwell and G. Herzberg, Laboratory Experiments on the Detectability of Silane (SiH_4) and Methyl Deuteride (CH_3D) in the Atmospheres of the Outer Planets, *Astrophys. J.*, 1953, **117**, 462.

74 R. G. Danehy, B. L. Lutz, T. Owen, T. W. Scattergood and W. Goetz, The absorption spectrum of monodeuterated methane (CH_3D) in the 6000–12 000 Å spectral region, *Astrophys. J.*, 1977, **213**, L139–L141.

75 Z. Lin, K. Boraas and J. P. Reilly, Analysys of an overtone band of CH_3D at 11 931 cm^{-1}, *J. Mol. Spectrosc.*, 1995, **170**(1), 266–278, DOI: **10.1006/jmsp.1995.1070**.

76 Y. Perez-Delgado, E. K. Lewis, C. J. Moehnke, M. C. Salazar, A. J. Hernandez and C. E. Manzanares, Cavity ring down absorption at low temperatures: C–H spectra (Δv = 1–6) of CH_3D and C–H overtones (Δv = 5, 6) of CH_2D_2 and CH_4, *Mol. Phys.*, 2009, **107**(13), 1367–1377, DOI: **10.1080/00268970902881987**.

77 J. L. Duncan and M. M. Law, Vibrational anharmonicity in dideuteromethane: a study of its infrared spectrum up to 17 000 cm^{-1}, *Spectrochim. Acta, Part A*, 1997, **53**(9), 1445–1457, DOI: **10.1016/S1386-1425(97)01815-5**.

78 L. F. H. Bovey, Rotation-Vibration spectra of diatomic and simple polyatomic molecules with long absorbing paths. X. The spectrum of trideuteromethane in the photographic infrared, *J. Chem. Phys.*, 1953, **21**, 830–836, DOI: **10.1063/1.1699043**.

79 A. Campargue and F. Stoeckel, Highly excited vibrational states of CHF_3 and CHD_3 in the range of the ν_5 = 5 CH chromophore, *J. Chem. Phys.*, 1986, **85**, 1220–1227, DOI: **10.1063/1.451259**.

80 A. Campargue, F. Stoeckel, M. Chenevier and H. Ben Kraiem, Rotational structure of overtone transitions of CHD_3 near 13 500 cm^{-1}, *J. Chem. Phys.*, 1987, **87**, 5598–5605, DOI: **10.1063/1.453531**.

81 M. Lewerenz and M. Quack, Vibrational spectrum and potential energy surface of the CH chromophore in CHD_3, *J. Chem. Phys.*, 1988, **88**, 5408–5432, DOI: **10.1063/1.454552**.

82 H. Ben Kraiem, A. Campargue, M. Chenevier and F. Stoeckel, Rotationally resolved overtone transitions of CHD_3 in the visible range, *J. Chem. Phys.*, 1989, **91**, 2148–2152, DOI: **10.1063/1.457022**.

83 A. Charvát, A. A. Kachanov, A. Campargue, D. Permogorov and F. Stoeckel, High sensitivity intracavity absorption spectroscopy of CHD_3 in the near infrared with a titanium: sapphire laser, *Chem. Phys. Lett.*, 1993, **214**(5), 495–501, DOI: **10.1016/0009-2614(93)85672-B**.

84 A. Campargue and D. Permogorov, Intracavity laser absorption spectroscopy of CHD_3 from 10 800 to 18 000 cm^{-1}, *J. Chem. Phys.*, 1994, **182**, 281–290, DOI: **10.1016/0301-0104(94)00043-3**.

85 D. Permogorov, A. Campargue, M. Chenevier and H. B. Kraiem, Rotational Analysis of Weak Overtone Transitions of CHD_3 between 10 800 and 17 500 cm^{-1}, *J. Mol. Spectrosc.*, 1995, **170**(1), 10–26, DOI: 10.1006/j.jms.1995.1053.

86 T. K. Ha, M. Lewerenz, R. Marquardt and M. Quack, Overtone intensities and dipole moment surfaces for the isolated CH chromophore in CHD_3 and CHF_3: Experiment and *ab initio* theory, *J. Chem. Phys.*, 1990, **93**, 7097–7109, DOI: 10.1063/1.459433.

87 R. Marquardt, M. Quack, J. Stohner and E. Sutcliffe, Quantum-mechanical wavepacket dynamics of the CH group in the symmetric top X_3CH compounds using effective hamiltonians from high-resolution spectroscopy, *J. Chem. Soc.*, 1986, **82**, 1173–1187, DOI: 10.1039/F29868201173.

88 R. Marquardt and M. Quack, Global analytical potential hypersurfaces for large amplitude motion and reactions in methane. II. Characteristic properties of the potential and comparison to other potentials and experimental information, *J. Phys. Chem. A*, 2004, **108**(15), 3166–3181, DOI: 10.1021/jp0373005v.

89 L. P. Giver, Intensity measurements of the CH_4 bands in the region 4350 Å to 10,600 Å, *J. Quant. Spectrosc. Radiat. Transfer*, 1978, **19**(3), 311–322, DOI: 10.1016/0022-4073(78)90064-X.

90 N. Bowles, R. Passmore, K. Smith, G. Williams, S. Calcutt and P. G. J. Irwin, Investigation of new band parameters with temperature dependence for self-broadened methane gas in the range 9000 to 14 000 cm^{-1} (0.71 to 1.1 μm), *J. Quant. Spectrosc. Radiat. Transfer*, 2012, **113**(10), 763–782, DOI: 10.1016/j.jqsrt.2012.03.001.

91 G. Pierre, J. C. Hilico, C. de Bergh and J. P. Maillard, The region of the $3\nu_3$ band of methane, *J. Mol. Spectrosc.*, 1980, **82**(2), 379–393, DOI: 10.1016/0022-2852(80)90122-8.

92 S. N. Yurchenko and J. Tennyson, ExoMol line lists - IV. The rotation–vibration spectrum of methane up to 1500 K, *J. Mon. Not. Royal Astron. Soc.*, 2014, **440**(2), 1649–1661, DOI: 10.1093/mnras/stu326.

93 T. Gherman and D. Romanini, Mode-locked cavity-enhanced absorption spectroscopy, *Opt. Express*, 2002, **10**(19), 1033–1042.

94 T. Gherman, S. Kassi, A. Campargue and D. Romanini, Overtone spectroscopy in the blue region by Cavity-Enhanced Broad-Band Absorption Spectroscopy with a modelocked femtosecond laser: application to acetylene, *Chem. Phys. Lett.*, 2004, **383**, 353–358, DOI: 10.1016/j.cplett.2003.10.148.

95 L. Rutkowski, P. Maslowski, A. C. Johansson and A. Khodabakhsh, Foltynowicz. Optical frequency comb Fourier transform spectroscopy with sub-nominal resolution and precision beyond the Voigt profile, *J. Quant. Spectrosc. Radiat. Transfer*, 2018, **204**, 63–73, DOI: 10.1016/j.jasrt.2017.09.001.

96 D. Charczun, A. Nishiyama, G. Kowzan, T. Cygan, T. Voumard, T. Wildi, T. Herr, V. Brash, D. Lisak and P. Maslowski, Dual-Comb cavity-mode and shift spectroscopy, *Measurement*, 2022, **188**, 110519, DOI: 10.1016/j.measurement.2021.110519.

97 M. Germann, A. Hjältén, V. Boudon, C. Richard, K. Krzempek, A. Hudzikowski, A. Gluszekc, G. Sobon and A. Foltynowicz, A methane line list with sub-MHz accuracy in the 1250 to 1380 cm^{-1} range from optical frequency comb Fourier transform spectroscopy, *J. Quant. Spectrosc. Radiat. Transfer*, 2022, **288**, 108252.

98 E. Baumann, F. R. Giorgetta, W. C. Swann, A. M. Zolot, I. Coddington and N. R. Newbury, Spectroscopy of the methane $\nu 3$ band with an accurate midinfrared coherent dual-comb spectrometer, *Phys. Rev. A: At., Mol., Opt. Phys.*, 2011, **84**, 062513, DOI: 10.1103/PhysRevA.84.062513.

99 A. M. Zolot, F. R. Giorgetta, E. Baumann, W. C. Swann, I. Coddington and N. R. Newbury, Broad-band frequency references in the near-infrared: Accurate dual comb spectroscopy of methane and acetylene, *J. Quant. Spectrosc. Radiat. Transfer*, 2013, **118**, 26–39, DOI: 10.1016/j.jqsrt.2012.11.024.

100 N. A. Malarich, D. Yun, K. Sung, S. Egbert, S. C. Coburn, B. J. Drouin and G. B. Rieker, Dual frequency comb absorption spectroscopy of CH_4 up to 1000 Kelvin from 6770 to 7570 cm^{-1}, *J. Quant. Spectrosc. Radiat. Transfer*, 2021, **272**, 107812, DOI: 10.1016/j.jqsrt.2021.107812.

101 A. Foltynowicz, T. Ban, P. Maslowski, F. Adler and J. Ye, Quantum-Noise-Limited Optical Frequency Comb Spectroscopy, *Phys. Rev. Lett.*, 2011, **107**, 233002, DOI: 10.1103/PhysRevLett.107.233002.

102 C. Gohle, B. Stein, A. Schliesser, T. Udem and T. W. Hansch, Frequency comb Vernier spectroscopy for broadband, high-resolution, high-sensitivity absorption and dispersion spectra, *Phys. Rev. Lett.*, 2007, **99**, 263902, DOI: 10.1103/PhysRevLett.99.263902.

103 L. Rutkowski and J. Morville, Broadband cavity-enhanced molecular spectra from Vernier filtering of a complete frequency comb, *Opt. Lett.*, 2014, **39**(23), 6664–6667, DOI: 10.1364/OL.39.006664.

104 C. Lu, J. Morville, L. Rutkowski, F. Senna Vieira and A. Foltynowicz, Cavity-Enhanced Frequency Comb Vernier Spectroscopy, *Photonics*, 2022, **9**(4), 222, DOI: 10.3390/photonics9040222.

105 L. Rutkowski and J. Morville, Continuous Vernier filtering of an optical frequency comb for broadband cavity-enhanced molecular spectroscopy, *J. Quant. Spectrosc. Radiat. Transfer*, 2017, **187**, 204–214, DOI: 10.1016/j.jqsrt.2016.09.021.

106 G. J. Scherer, K. K. Lehmann and W. Klemperer, The high-resolution visible overtone spectrum of CH_4 and CD_3H at 77K, *J. Chem. Phys.*, 1984, **81**, 5319–5325, DOI: 10.1063/1.447674.

107 M. Rey, A. V. Nikitin and Vl Tyuterev, Theoretical hot methane line list up to T = 2000 K for astrophysical applications, *Astrophys. J.*, 2014, **789**, 2, DOI: 10.1088/0004-637X/789/1/2.

108 M. Rey, A. V. Nikitin and Vl Tyuterev, Accurate theoretical methane line lists in the infrared up to 3000 K and quasi-continuum absorption/emission modeling for astrophysical applications, *Astrophys. J.*, 2017, **847**, 105, DOI: 10.3847/1538-4357/aa8909.

109 R. J. Hargreaves, P. F. Bernath, J. Bailey and M. Dulick, Empirical line list and absorption cross sections for methane at high temperatures, *Astrophys. J.*, 2015, **813**(1), 12, DOI: 10.1088/0004-637X/813/1/12.